Modulatory features of the novel spider toxin μ-TRTX-Df1a isolated from the venom of the spider *Davus fasciatus*.

Running title: Modulation of voltage-gated channels by the spider toxin Df1a

Fernanda C Cardoso[a]*, Zoltan Dekan[a], Jennifer J Smith[a], Jennifer R Deuis[a,b], Irina Vetter[a,b], Volker Herzig[a], Paul F Alewood[a], Glenn F King[a] and Richard J. Lewis[a]*.

[a]Institute for Molecular Bioscience, The University of Queensland, St Lucia, Qld 4072, AU.

[b]School of Pharmacy, The University of Queensland, Woolloongabba, Qld 4102, AU.

Corresponding authors*: Prof Richard J. Lewis, 306 Carmody Rd, St Lucia, Qld 4072, Australia. Phone: +61 7 3346 2984, e-mail: r.lewis@uq.edu.au; Dr Fernanda C. Cardoso, 306 Carmody Rd, St Lucia, Qld 4072, Australia. Phone: +61 7 3346 2986, e-mail: f.caldascardoso@uq.edu.au.

Number of figures: 9

Number of tables: 1

Supporting information: 3

This article has been accepted for publication and undergone full peer review but has not been through the copyediting, typesetting, pagination and proofreading process which may lead to differences between this version and the Version of Record. Please cite this article as doi: 10.1111/bph.13865

Abstract

Background and purpose

Naturally occurring dysfunction in Na_V channels results in complex disorders such as chronic pain, making these channels an attractive target for new therapies. In the pursuit of novel Na_V modulators, we investigated spider venoms for new inhibitors of Na_V channels.

Experimental Approach

We used high-throughput screens to identify a Na_V modulator in venom of the spider *Davus fasciatus*. Further characterization of this venom peptide was undertaken using fluorescent and electrophysiological assays, molecular modeling and a rodent pain model.

Key Results

We identified a potent Na_V inhibitor named μ-TRTX-Df1a. This 34-residue peptide fully inhibited responses mediated by $Na_V1.7$ endogenously expressed in SH-SY5Y cells. Df1a also inhibited Ca_V3 currents but had no activity against K_V2. The modelled structure of Df1a, which contains an inhibitor cystine knot motif, is reminiscent of the Na_V channel toxin ProTx-I. Electrophysiology revealed that Df1a inhibits all Na_V subtypes tested ($hNa_V1.1$–1.7). Df1a also slowed fast inactivation of $Na_V1.1$, $Na_V1.3$ and $Na_V1.5$, and modified the voltage-dependence of activation and inactivation of most Na_V subtypes. Df1a preferentially binds to the domain II voltage-sensor and has additional interactions with the voltage sensors domains III and IV, which likely explains its modulatory features. Df1a was analgesic *in vivo,* reversing the spontaneous pain behaviors induced by the Na_V activator OD1.

Conclusion and Implication

μ-TRTX-Df1a shows potential as a new molecule for the development of therapies to treat voltage-gated ion channels mediated pain disorders.

Abbreviations: ACN, acetonitrile; Ca_V, voltage-gated calcium channel; DIEA, N, N-diisopropylethylamine; DMF, N, N-dimethylformamide; FLIPR, Fluorescence imaging plate reader; HBTU, 2-(1H-benzotriazol-1-yl)-1,1,3,3-tetramethyluronium hexafluorophosphate; ICK, inhibitor cysteine knot; K_V, voltage-gated potassium channel; Na_V, voltage-gated sodium channel; MALDI-TOF, Matrix-assisted laser desorption/ionization time of flight; RP-HPLC, reversed-phase high-performance liquid chromatography; TFA, trifluoroacetic acid; TIPS, triisopropylsilane.

Pharmacological nomenclature

Targets: Ca_V3.1, Ca_V3.2, Ca_V3.3, K_V2.1, Na_V1.1, Na_V1.2, Na_V1.3, Na_V1.4, Na_V1.5, Na_V1.6, Na_V1.7, Na_V1.8 and Na_V1.9.

Ligands: Veratridine.

1. Introduction

Animal venoms have evolved into potent neurotoxins for predation and defense that cause harmful neurologic alterations in insects and mammals (King & Hardy, 2013; Klint et al., 2012). These effects are induced by molecules acting on ion channels involved in the generation and transmission of electrical signals in neurons and muscles, which play a key role in several biological processes. The potency and ion channel selectivity of these neurotoxins have made them powerful pharmacological tools as well as therapeutic leads for treating channelopathy-related disorders. These include conditions such as neuropathic pain, epilepsy and arrhythmia, which often involve dysfunction of voltage-gated sodium (Na_V) channel (Catterall et al., 2010; Remme & Bezzina, 2010; Rogers et al., 2006).

Na_V channels are glycosylated transmembrane proteins involved in action potential generation and propagation in excitable cells. In mammals, the Na_V channel family is composed of nine subtypes (Na_V1.1–Na_V1.9) that differ in their α-subunit sequences and their pharmacological and functional properties. Alterations in Na_V channel function and/or expression underlines a variety of disorders including chronic pain (Lauria et al., 2014; Moldovan et al., 2013). In particular, Na_V1.3, Na_V1.7, Na_V1.8 and Na_V1.9 have been strongly implicated in chronic pain (Liu & Wood, 2011). Expression of Na_V1.3, Na_V1.8 and Na_V1.9 is altered during neuropathic pain (Dib-Hajj et al., 1999), while individuals lacking Na_V1.7

function exhibit a congenital insensitivity to pain, with no other sensory abnormalities apart from anosmia (Cox et al., 2006). Several epileptic conditions are due to mutation or altered expression of $Na_V1.1$ and $Na_V1.2$ (Meisler & Kearney, 2005), and numerous anticonvulsants act on Na_V channels by stabilizing their fast inactivation or slow-inactivated states (Errington et al., 2008; Ragsdale & Avoli, 1998). Other conditions such as congenital paramytonia and Brugada syndrome also present alterations in Na_V channels ($Na_V1.4$ and $Na_V1.5$, respectively) (Amin et al., 2010; Zhao et al., 2012). Thus, Na_V channels are common targets for the development of drugs to treat complex disorders.

Several neurotoxins sourced from animal venoms have been described as modulators of Na_V channels (Herzig et al., 2011; Kaas et al., 2012). Most have high potency at Na_V channels but lack selectivity for the relevant therapeutic targets and cause side effects and even death at low doses. Spider-venom peptides have shown promising selectivity for Na_V subtypes involved in pain pathways (Klint et al., 2015) and they have been used as leads in the search for new analgesics. Using fluorescence assays and either endogenously or heterologously expressed Na_V subtypes (Cardoso et al., 2015; Vetter et al., 2012), we have begun to systematically identify and characterize peptidic Na_V channel modulators from spider crude venoms. In the present work, we describe the isolation and characterization of a new ion channel inhibitor (Df1a) from the tarantula *Davus fasciatus* using a high-throughput fluorescence screen. Df1a (μ-TRTX-Df1a) potently inhibits hNa_V and hCa_V3 channels. Interestingly, Df1a displays a novel dual modulation for specific hNa_V subtypes, simultaneously inhibiting peak current and slowing fast inactivation, and reversed pain behaviors induced by intraplantar OD1 activation of Na_V in mice.

2. Material and Methods

2.1 Animals

For behavioral assessment, we used adult male C57BL/6J mice aged 6–8 weeks weighing 20–25 g. Mice were housed in groups of 3–4 per cage, under 12 h light-dark cycle, with standard rodent chow and water provided *ad libitum*.

2.2 Ethics Statement

Ethical approval for *in vivo* experiments was obtained from The University of Queensland Animal Ethics Committee (AEC Approval Number IMB/PACE/326/15). Experiments involving animals were conducted in accordance with the Animal Care and Protection Regulation Qld (2012), the *Australian Code of Practice for the Care and Use of Animals for Scientific Purposes*, 8th edition (2013) and the *International Association for the Study of Pain Guidelines for the Use of Animals in Research*.

2.3 Cell culture

The human neuroblastoma cell line SH-SY5Y was maintained at 37°C in a humidified 5% CO_2 incubator in Roswell Park Memorial Institute (RPMI) medium supplemented with 15% fetal bovine serum (FBS) and 2 mM L-glutamine. Human Embryonic Kidney (HEK 293) cells expressing recombinant hNa_V subtypes co-expressed with β1 auxiliary subunits (SB Drug Discovery, Glasgow, UK) were maintained at 37°C in a humidified 5% CO_2 incubator in Minimal Essential medium supplemented with 10% FBS, 100 units mL^{-1} penicillin and 100 μg mL^{-1} streptomycin, 2 mM L-glutamine and variable concentrations of blasticidin, geneticin and zeocin according to manufacturer's protocols. Replicating cells were sub-cultured every 3–4 days in a 1:5 ratio using 0.25% trypsin/EDTA. Chinese hamster ovarian (CHO) cells expressing recombinant $hNa_V1.6$ channels (EZ cells, ChanTest Corp, OH, USA) were maintained at 37°C in a humidified 5% CO_2 incubator in F-12 medium supplemented with 10% FBS, 100 U mL^{-1} penicillin and 100 μg mL^{-1} streptomycin.

2.4 Venom fractionation

Venom from *Davus fasciatus* was obtained by electrical stimulation as previously described (Herzig & Hodgson, 2009). Dried venom (1 mg) was dissolved in 100 μl Milli-Q water containing 0.05% trifluoroacetic acid (TFA) (Auspep, VIC, AU) and 5% acetonitrile (ACN) and centrifuged at 14,000 rpm for 10 min to remove particulates. Venom was fractionated by reversed-phase high performance liquid chromatography (RP-HPLC) using a C18 column (Vydac 4.6 mm x 250 mm, 5 μm, Grace Discovery Sciences, USA) with a gradient of solvent B (90% ACN in 0.045% TFA) in solvent A (0.05% TFA). The gradient was 5% B for 5 min, followed by 20 to 40% solvent B over 60 min at a flow rate 0.7 mL min^{-1}. Peaks were collected at 0.7 mL per well and fractions were lyophilized before storage at –20°C.

2.5 Screening against $hNa_V1.7$

Venom fractions were screened for inhibition of $hNa_V1.7$ as previously described (Cardoso et al., 2015). Briefly, SH-SY5Y cells were plated at 40,000 cells per well in 384-well flat clear-bottom black plates (Corning, NY, USA) and cultured at 37°C in a humidified 5% CO_2

incubator for 48 h. Cells were loaded with 20 µl per well Calcium 4 dye (Molecular Devices) reconstituted in assay buffer containing (in mM) 140 NaCl, 11.5 glucose, 5.9 KCl, 1.4 $MgCl_2$, 1.2 NaH_2PO_4, 5 $NaHCO_3$, 1.8 $CaCl_2$ and 10 HEPES pH 7.4 and incubated for 30 min at 37°C in a humidified 5% CO_2 incubator. Fluorescence responses were recorded using excitation at 470–495 nm and emission at 515–575 nm for 10 s to set the baseline, then 600 s after addition of 10% venom fraction/well and for a further 300 s after co-addition of 3 µM veratridine and 30 nM OD1.

2.6 Mass spectrometry and peptide sequencing

Peptide masses were determined by matrix-assisted laser desorption ionization-time of flight mass spectrometry (MALDI-TOF MS) using a 4700 Proteomics Bioanalyser Model (Applied Biosystems, CA, USA). Df1a was dissolved in water mixed 1:1 (v/v) with α-cyano-4-hydroxy-cinnamic acid matrix (7 mg mL^{-1} in 50% ACN) and mass spectra acquired in positive reflector mode. The reported molecular weight of Df1a is for the monoisotopic $M+H^+$ ion. N-terminal sequencing was outsourced to the Australian Proteome Analysis Facility, Sydney, Australia. Briefly, the peptide was dissolved in urea (4 M) and ammonium bicarbonate (50 mM) and reduced with dithiothreitol (100 mM) at 56°C for 1 h under argon. The sample was then alkylated using acrylamide (220 mM) for 0.5 h in the dark. The reaction was quenched by the addition of excess dithiothreitol. After desalting by RP-HPLC, the collected fraction was loaded onto pre-cycled bioprene discs and subjected to 34 cycles of Edman degradation N-terminal sequencing using an ABI 494 Procise Protein Sequencing System (Applied Biosystems).

2.7 Solid phase synthesis of Df1a

Solvents for RP-HPLC consisted of 0.05% TFA/H_2O (Solvent A) and 90% ACN/0.043% TFA/H_2O (Solvent B). Analytical HPLC was performed on a Shimadzu LC20AT system using a Thermo Hypersil GOLD 2.1 x 100 mm C18 column heated at 40°C with a flow rate of 0.3 mL min^{-1} and a gradient of 10 to 55% B over 30 min unless otherwise stated. The eluent was monitored at 214 nm unless otherwise stated. Preparative HPLC was performed on a Vydac 218TP1022 column running at a flow rate of 16 mL min^{-1} using a gradient of 10 to 50% B over 40 min. Mass spectrometry was performed on an API2000 (ABI Sciex) mass spectrometer in positive ion mode. Df1a-NH_2 and Df1a-OH were chain assembled on a Symphony (Protein Technologies Inc., AZ, USA) automated peptide synthesizer on Rinkamide (loading 0.67 mmol g^{-1}) and Fmoc-Phe-Wang (loading 0.70 mmol g^{-1}) polystyrene resins, respectively, on a 0.1 mmol scale. Fmoc deprotections were achieved using 30% piperidine DMF (1 × 1.5 min, then 1 × 4 min). Couplings was performed in DMF using 5 equivalents of Fmoc-amino acid/HBTU/DIEA (1:1:1) relative to resin loading for 2 × 20 min. Amino acid side-chains were protected as follows: Asp(OtBu), Arg(Pbf), Cys(Trt), Gln(Trt), Glu(OtBu), His(Trt), Lys(Boc), Ser(tBu), Thr(tBu), Trp(Boc). Cleavage from the resin and removal of side-chain protecting groups was achieved by treatment with 95% TFA/2.5% TIPS/2.5% H_2O at room temperature for 2 h. After most of the cleavage solution was evaporated under a stream of N_2, the products were precipitated and washed with cold Et_2O and lyophilized from 50% ACN / 0.1% TFA / H_2O. Df1a-NH_2: 192 mg; ESI-MS (*m/z*): calc. (avg) 1362.6 Da $[M+3H]^{3+}$, found 1362.3 Da. The crude product was purified by preparative HPLC to give 50 mg of hexathiol Df1a-NH_2. Df1a-OH: 204 mg; ESI-MS (*m/z*): calc. (avg) 1362.9 Da $[M+3H]^{3+}$, found 1362.7 Da. The crude product was purified by preparative HPLC to give 50 mg of hexathiol Df1a-OH.

2.8 Oxidative folding

Purified reduced peptide (10 mg of Df1a-NH_2 or Df1a-OH), reduced glutathione (100 equiv.) and oxidized glutathione (10 equiv.) were dissolved in 6M guanidine HCl (33 mL) then added to a solution of 0.1 M Tris (pH 8.0, 67 mL) and stirred at 4°C with exposure to air for 4 days. The major products were isolated by preparative HPLC. Df1a-NH_2: 2.9 mg; ESI-MS (*m/z*): calc. (avg) 1360.6 Da $[M+3H]^{3+}$, found 1360.4 Da. Df1a-OH: 2.5 mg; ESI-MS (*m/z*): calc. (avg) 1360.9 Da $[M+3H]^{3+}$, found 1360.5 Da.

2.9 Patch-clamp electrophysiology in mammalian cells

Na_V channels experiments were recorded in HEK 293 (SB Drug Discovery) cells expressing specific hNa_V subtypes co-expressed with the β1 auxiliary subunit or CHO expressing hNa_V subtypes (EZ cells, ChanTest Corp) and Na^+ currents measured by whole-cell patch clamp using the automated system QPatch 16X (Biolin Scientific A/S, Ballerup, Denmark). The extracellular solution comprised (in mM) 1 $CaCl_2$, 1 $MgCl_2$, 5 HEPES, 3 KCl, 140 NaCl, 0.1 $CdCl_2$ and 20 TEA-Cl at pH 7.3 and 320 mOsm, and the intracellular solution comprised (in mM) 140 CsF, 1/5 EGTA/CsOH, 10 HEPES and 10 NaCl at pH 7.3 and 320 mOsm. The elicited currents were sampled at 25 kHz and filtered at 4 kHz. The average seal, whole-cell and chip resistances values were (in MΩ) 3690, 997 and 2.08, respectively. Cells with less than 1 nA of peak Na^+ current were not used in this study. Cells were maintained at a holding potential –80 mV and Na^+ currents elicited by 20 ms voltage steps to 0 mV from a –120 mV conditioning pulse applied for 200 ms. To obtain concentration–response curves, cells were incubated for 5 min with increasing concentrations of Df1a. For on-rate experiments, Na^+ currents were measured at 15 s intervals over 15 min immediately following addition of Df1a at correspondent IC_{50} and 10x IC_{50} concentrations for the Na_V subtypes analyzed. For off-rate measurements, cells were incubated for 10 min with Df1a at correspondent IC_{50} concentrations for the Na_V subtypes analyzed and Na^+ currents assessed at 5-min intervals during saline washes. The K_{on}, K_{off} and K_d were calculated using $K_d = K_{off}/K_{on}$ (nM), where $K_{off} = 1/\tau_{off}$ (s^{-1}) and $K_{on} = (1/\tau_{on} - K_{off})/[toxin]$ ($nM^{-1}S^{-1}$). Voltage-activation relationships were obtained by measuring steady-state Na^+ currents elicited by step depolarizations from –110 to +80 mV using 10 mV increments. The peak conductance (G_{Na}) was calculated from $G = I/(V-V_{rev})$, where I, V and V_{rev} represent the current value, membrane potential and reverse potential, respectively. The voltage of steady-state fast inactivation was estimated using a double-pulse protocol with currents elicited by a 20 ms depolarizing potential of 0 mV following a 500 ms pre-pulse to potentials from –130 to –10 mV using 10 mV increments. Voltage-dependence of activation and inactivation relationships was examined either in the absence and presence of Df1a (5 min exposure) with the cells before application of the voltage protocols. Ca_V3 channels experiments were recorded in CHO cells expressing $hCa_V3.1$ and HEK 293 cells expressing $hCa_V3.2$ and $hCa_V3.3$ (these cell lines were kindly donated by Prof Emmanuel Bourinet from the Institute of Functional Genomics, Montpellier University, FR and Prof Edward Perez-Reyes from the School of Medicine, University of Virginia, USA) and Ca^{+2} currents measured by whole-cell patch clamp using an automated system QPatch 16X. The extracellular solution comprised (in mM) 5 $CaCl_2$, 0.5 $MgCl_2$, 10 HEPES and 157 TEA-Cl at pH 7.3 and 320 mOsm, and the intracellular solution comprised (in mM) 140 CsF, 1 EGTA, 10 HEPES and 10 NaCl at pH 7.3 and 320 mOsm. The elicited currents were sampled at 25 kHz and filtered at 4 kHz. The average seal, whole-cell and chip resistances values were (in MΩ) 5000, 1953 and 2.2 for CHO and 1536, 734 and 2.1 for HEK 293, respectively. Cells were maintained at a holding potential –90 mV and Ca^{+2} currents elicited by 60 ms voltage steps to -30 mV from a –120 mV conditioning pulse applied for 60 ms. To obtain concentration–response curves, cells were incubated for 5 min with increasing concentrations of Df1a. All experimental data was analyzed using QPatch Assay Software v5.0 (Biolin Scientific A/S).

2.10 Determination of Df1a binding sites on $hNa_V1.7$

$hNa_V1.7/rK_V2.1$ chimeras containing the S3 and S4 loop and helices of the $hNa_V1.7$ paddle were generated previously (Klint et al., 2015). *Xenopus laevis* oocytes were injected with cRNA encoding $hNa_V1.7/rK_V2.1$ chimera or $rK_V2.1$. Two-electrode voltage clamp electrophysiology (Axoclamp 900A, Molecular Devices; 40 μL recording chamber) was used to measure currents 1–4 days after cRNA injection and incubation at 17°C in ND96 that contained (in mM) 96 NaCl, 2 KCl, 5 HEPES, 1 $MgCl_2$, 1.8 $CaCl_2$ and 50 μg mL^{-1} gentamycin, pH 7.6. Data were filtered at 4 kHz and digitized at 20 kHz using pClamp software (Molecular Devices). Micro-electrode resistances were 0.5–1 MΩ when filled with 3 M KCl. The external recording solution contained (in mM) 50 KCl, 50 NaCl, 5 HEPES, 1 $MgCl_2$, 0.3 $CaCl_2$, pH 7.6 with NaOH. Experiments were performed at room temperature (~22 °C). Toxin samples were diluted in recording solution with 0.1% BSA. Potassium currents were elicited by depolarization to +70 mV from a holding potential of –90 mV (–120 mV for the DIII chimera), with a tail voltage at –60 mV (–90 mV for the DIII chimera). Leak and background conductance, identified by blocking channels with agitoxin-2, were subtracted for all experiments.

2.11 Activity of Df1a in vivo

The efficacy of Df1a to inhibit Na_V induced pain *in vivo* was assessed in mice using the α-scorpion toxin OD1 as previously described (Cardoso et al., 2015; Deuis et al., 2016). To induce spontaneous pain behaviors, the Na_V activator OD1 (300 nM) ± Df1a-OH (10 μM, 1 μM) or Df1a-NH_2 (10 μM, 1 μM) was administered by intraplantar injection into the left hind paw of mice in phosphate buffered saline containing 0.1% BSA and volume of 40 μL under 2% isoflurane anaesthesia. Mice were then placed individually into Perspex boxes (10 × 10 × 10 cm) and the number of spontaneous pain behaviors (licks and flinches) was counted by an observer unaware of the treatments received for 10 min following injection of OD1 from video recordings.

2.12 Molecular model of Df1a

The three dimensional structure of Df1a was modeled using the NMR-derived structure of β/ω-theraphotoxin-Tp1a (ProTx-I, PDB code 2M9L) as template (Gui et al., 2014). Backbone fitting and energy minimization were performed using the Swiss-Model prediction algorithm (open source, http://swissmodel.expasy.org) (Arnold et al., 2006) and displayed using the

PyMOL Software package (DeLano, 2002). The model was validated by inspection of the Ramachandran plot (Lovell et al., 2003).

2.13 Data analysis

The data and statistical analysis comply with the recommendations on experimental design and analysis in pharmacology (Curtis et al., 2015). Curve fitting was achieved using GraphPad Prism Version 6 (GraphPad Software Inc, San Diego, CA, USA) using nonlinear regression with log[inhibitor] versus normalized response and variable Hill slope for dose-responses, Boltzmann sigmoidal equation for voltage-dependence of activation and inactivation and exponential one-phase association for on and off-rate analysis. Data were represented as mean ± SEM of at least five independent experiments, unless otherwise stated. For the *in vitro* experiments, statistical significance was determined by paired *t*-test assuming equal variance. For the *in vivo* experiments, statistical significance was determined by ANOVA with Dunnett's post-test. $P < 0.05$ was considered significant.

2.14 Materials

Cell culture reagents were from Gibco, Life Technologies Corporation (Carlsbad, CA, USA), unless otherwise stated. For the RP-HPLC, calcium influx assays, peptide synthesis and oxidative folding, electrophysiological assays and *in vivo* experiments, all reagents were from Sigma-Aldrich (St Louis, MO, USA) unless otherwise stated.

2.15 Nomenclature of Targets and Ligands

Key protein targets and ligands in this article are hyperlinked to corresponding entries in http://www.guidetopharmacology.org, the common portal for data from the IUPHAR/BPS Guide to PHARMACOLOGY (Southan et al., 2016), and are permanently archived in the Concise Guide to PHARMACOLOGY 2015/16 (Alexander et al., 2015).

3. Results

3.1 Peptide toxin identification and chemical synthesis

Fractionation of the *Davus fasciatus* venom (1 mg) using RP-HPLC revealed eight dominant peaks eluting from 20% to 40% solvent B (Figure 1A). Testing aliquots (10%) of 1-min fractions for activity in SH-SY5Y cells stimulated by co-addition of OD1 and veratridine revealed three fractions that strongly inhibited $hNa_V1.7$ (Figure 1A, gray circles). MALDI-

TOF MS analysis revealed that the peaks eluting at 30.8 and 32.2 min contained multiple peptides that proved difficult to separate and could not be definitively characterized (data not shown). The remaining fraction eluting at 36–37 min (33% B) contained a single major peptide with a monoisotopic mass of 4075.8 Da (Figure 1B). N-terminal Edman sequencing disclosed a novel 34-residue peptide that we named Df1a (μ-TRTX-Df1a). The peptide sequence had a calculated monoisotopic oxidized mass of 4076.8 Da, suggesting that it was C-terminally amidated in its native form (Figure 1C). Sequence comparisons revealed that Df1a belonged to the Family 2 of Na_V-targeting spider toxins (NaSpTx), which is comprised of 33–41 residues peptides with hyper-stable ICK motifs that inhibit Na_V, Ca_V and K_V channels (Herzig & King, 2015; Klint et al., 2012). Sequence analysis revealed the highest identity with β/ω-TRTX-Tp1a (ProTx-I, 73%), ω-TRTX-Hhn1a (64%) and TRTX-Hh2a (61%) (Figure 1D).

Chemical synthesis was used to generate the C-terminal amide and acid forms of Df1a (Figure 2A). Both native and synthetic Df1a-NH_2, as well as synthetic Df1a-OH, eluted as a complex set of partially resolved peaks by analytical HPLC at 40°C (Figure 2A) but as two peaks at 23°C (Figure 2B). Comparable temperature-dependent dynamics have been reported previously for human β-defensins (Chino et al., 2006), while hanatoxin also elutes as two peaks, although temperature dependence was not reported (Takahashi et al., 2000). Importantly, all major peaks associated with synthetic Df1a-NH_2 co-eluted with native Df1a, confirming the assigned sequence and that the native disulfide bond pairings had been achieved. In order to rapidly evaluate the activity of the synthetic Df1a over Na_V channels, a FLIPR-based fluorescence assay was performed. Synthetic Df1a-NH_2 was found to potently inhibit endogenous $hNa_V1.7$ in SH-SY5Y cells (Figure 2C). Given their structural identity and functional activity, synthetic Df1a (sDf1a-NH_2 and sDf1a-OH) was used for all subsequent characterization studies.

3.2 Effect of Df1a on Na_V channels and Ca_V3

We evaluated the effect of Df1a on a range of voltage-gated ion channels by using automated whole-cell patch clamp to examine its effect on $hNa_V1.1$–1.5, $hNa_V1.7$, $hCa_V3.2$ and $hCa_V3.3$ expressed in HEK 293 cells, and $hNa_V1.6$ and $hCa_V3.1$ expressed in CHO cells (Figure 3 A–J, Supporting Information Table S1). Df1a-NH_2 inhibited $hNa_V1.1$–1.7 channels, with preference for $hNa_V1.2$, $hNa_V1.3$ and $hNa_V1.7$. The C-terminal acid form of Df1a (Df1a-OH) lost potency at all Na_V subtypes compared the C-terminal amide form, especially at $hNa_V1.7$, to be $hNa_V1.2$, $hNa_V1.3$ and $hNa_V1.6$ preferring. The effect of Df1a was also investigated by two-electrode voltage clamp in *Xenopus laevis* oocytes expressing $hNa_V1.7$ showing Df1a-NH_2 inhibited this channel with more potency compared to Df1a-OH, and displayed IC_{50} values of up to 8.5-fold difference compared to the automated whole-cell patch clamp in mammalian cells (Supporting Information Fig. S1A and S1C). Furthermore, the effect of ProTx-I, a spider toxin also belonging to the NaSpTx Family 2, was investigated on $hNa_V1.7$ by two-electrode voltage clamp and automated whole-cell patch clamp. ProTx-I inhibited $hNa_V1.7$ currents with similar IC_{50} values in both electrophysiology systems (Supporting Information Fig. S1E and Fig. S2A). Df1a-NH_2 also inhibited the Ca_V3 channels responses, with preference for $hCa_V3.1$ and $hCa_V3.3$. This inhibition was less potent in the C-terminal acid form of Df1a for all Ca_V3 subtypes. The IC_{50} values and Hill slope for each hNa_V and hCa_V3 subtypes in the presence of Df1a are described in Supporting Information Table S1. The number of independent experiments are indicated in Supporting Information Table S1.

3.3 Effect of Df1a on activation and inactivation of hNa_V channels

Most spider toxins that inhibit Na_V channels are gating modifiers that alter the voltage-dependence of channel gating (Catterall et al., 2007). In order to investigate the mode of action of Df1a, we examined its effect on the voltage-dependence of Na_V channel activation and steady state-inactivation using automated whole-cell patch clamp using HEK293 cells expressing the $hNa_V1.1$–1.5 and 1.7, and CHO cells expressing $hNa_V1.6$. We found that both Df1a-NH_2 and Df1a-OH shifted the voltage-dependence of activation and of steady-state fast inactivation of hNa_V subtypes to more hyperpolarizing or depolarizing potentials when applied at respective IC_{50} concentration for each Na_V channel subtype (Figure 4). More specifically, Df1a considerably altered the voltage-dependence of activation of $hNa_V1.2$ (ΔV_{50} (*mV*) –6.9 ± 1.3 for Df1a-OH), $hNa_V1.3$ (ΔV_{50} (*mV*) 10.6 ± 1.6 and 5.6 ± 1.3 for Df1a-NH_2 and OH, respectively), $hNa_V1.5$ (ΔV_{50} (*mV*) –7.2 ± 2.1 for Df1a-OH) and $hNa_V1.7$ (ΔV_{50} (*mV*) 10.7 ± 1 and 5.3 ± 1.5 for Df1a-NH_2 and OH, respectively) (Figure 4 B, C, E and G). Moreover, Df1a shifted the voltage-dependence of steady-state fast inactivation of $hNa_V1.1$ (ΔV_{50} (*mV*) –19.1 ± 2.6 for Df1a-NH_2), $hNa_V1.2$ (ΔV_{50} (*mV*) –9.1 ± 2.2 and –5.3 ± 1.3 for Df1a-NH_2 and OH, respectively), $hNa_V1.6$ (ΔV_{50} (*mV*) –6.5 ± 0.98 and –8 ± 2.6 for Df1a-NH_2 and OH, respectively) and $hNa_V1.7$ (ΔV_{50} (*mV*) –16.9 ± 2.9 and –17.5 ± 2.3 for Df1a-NH_2 and OH, respectively) (Figure 4A, B, D and F). In striking contrast, Df1a shifted the steady-state inactivation for $hNa_V1.3$ to more depolarizing potentials (ΔV_{50} (mV) 9.6 ± 1.5 and 7.9 ± 2.3 for Df1a-NH_2 and OH, respectively) (Figure 4C). ΔV_{50} values not reported were between –5 mV and +5mV. There was a general trend for Df1a to shift both voltage-dependence of activation and of steady-state fast inactivation of the hNa_V subtypes to more hyperpolarizing potentials, with exemptions found for the subtypes $hNa_V1.3$ and $hNa_V1.7$ (Figure 4H). The effect of Df1a on activation and inactivation of $hNa_V1.7$ was also investigated by two-electrode voltage clamp in *Xenopus laevis* oocytes (Supporting Fig. S1B and S1D). No effect in the voltage-dependence of activation and inactivation of $hNa_V1.7$ was observed in the presence of Df1a-NH_2 and Df1a-OH when two-electrode voltage clamp in oocytes was used. A similar effect in $hNa_V1.7$ was observed in the presence of ProTx-I, where there were no significant changes in the voltage-dependence of activation and inactivation using both two-electrode voltage clamp and automated whole-cell patch clamp electrophysiology systems (Supporting Fig. S1F and Fig. S2B).

A slowing in the fast inactivation of Na_V channels was observed for $hNa_V1.1$, $hNa_V1.3$ and $hNa_V1.5$ in the presence of Df1a-NH_2 and Df1a-OH (Figure 5). Representative traces show slowed fast inactivation occurring simultaneously with peak current inhibition in the presence of Df1a at the respective IC_{50} concentrations for each channel subtype (Figure 5A). The slowing in fast inactivation was fully inhibited in the presence of 1 μM Df1a, along with peak current. The inactivation decay time constant (τ) was calculated, revealing this toxin slows the inactivation of $Na_V1.1$ by 2.1 and 2.3-fold, $Na_V1.3$ by 36.2 and 9-fold and $Na_V1.5$ by 2.1 and 1.8-fold in the presence of Df1a-NH_2 and Df1a-OH, respectively. The remaining fraction of currents was calculated at 20 ms after 0 mV application, showing $Na_V1.3$ with the highest fraction of persistent currents, followed by $Na_V1.5$ and $Na_V1.1$. (Figure 5B–D).

3.4 Kinetics of Df1a inhibition and current recovery in $hNa_V1.3$ and $hNa_V1.7$

Association/dissociation rates and reversibility can impact considerably on the therapeutic potential of ion channel modulators. Thus, we used automated whole-cell patch clamp electrophysiology to measure on- and off-rates for Df1a inhibition of $hNa_V1.3$ and $hNa_V1.7$. Current inhibition and recovery were estimated following application of the amidated and acid forms of Df1a (Figure 6A-H, Table 1). The association rates for $hNa_V1.3$ (K_{on}) were slower for Df1a-NH_2 compared to Df1a-OH at IC_{50} values (τ (min) 3.92 and 1.51 for Df1a-NH_2 and Df1a-OH, respectively) (Figure 6A), while for $hNa_V1.7$ the association rates (K_{on})

were faster for the Df1a-NH_2 compared to Df1a-OH at IC_{50} values (τ (min) 0.64 and 3.06 for Df1a-NH_2 and Df1a-OH, respectively) (Figure 6B). When applied at concentration ten times the respective IC_{50} value, Df1a-OH showed faster association rates for both $hNa_V1.3$ and $hNa_V1.7$. Current traces after 2.5 min incubation with Df1a showed a persistent slowing in fast inactivation for $hNa_V1.3$, which was absent in $hNa_V1.7$ (Figure 6C–F). The inhibition of $hNa_V1.3$ and $hNa_V1.7$ was quasi-irreversible for Df1a-NH_2, while for Df1a-OH the inhibition was quasi-irreversible for $hNa_V1.7$ but reversible for $hNa_V1.3$ (Figure 6G and H). The irreversibility of Df1a was tested using a –80 mV holding potential, and more hyperpolarized holding potentials should be tested in the near future to further evaluate irreversibility of this toxin over Na_V channels.

3.5 $Na_V1.7$ sites interacting with Df1a

We used a panel of previously described $hNa_V1.7/rK_v2.1$ S3-S4 paddle chimeras (Klint et al., 2015) to map the binding site for Df1a on $hNa_V1.7$ (Figure 7). The acid and amide forms of Df1a had no effect on the DI chimera or wild-type $rK_V2.1$ at 1 μM concentration, and they only partially inhibited currents from the DIII and DIV chimeras. In contrast, 1 μM Df1a-NH_2 and Df1a-OH significantly inhibited currents from the DII chimera. Thus, our data indicate that Df1a primarily interacts with the DII voltage sensor of $hNa_V1.7$, with weaker interactions with VSD III and IV.

3.6 Df1a is analgesic in a mouse model of pain

In order to evaluate the potential of Df1a to reverse peripheral pain *in vivo*, we use an OD1-induced pain model. Intraplantar injection of OD1, a scorpion toxin that preferentially potentiates $Na_V1.4$, $Na_V1.6$ and $Na_V1.7$ (Durek et al., 2013), causes rapid development of spontaneous pain in mice as evidenced by flinching and licking of the affected hind paw (Cardoso et al., 2015; Deuis et al., 2016). Intraplantar injection of 10 μM Df1a-NH_2 or Df1a-OH (400 pmoles in a 40 μl injection) significantly reduced spontaneous pain behavior (Figure 8; OD1, 102 ± 4 flinches 10 min^{-1}; 10 μM Df1a-NH_2, 56 ± 7 flinches 10 min^{-1}; 1 μM Df1a-OH, 73 ± 8 flinches 10 $min^{-}1$; 10 μM Df1a-OH, 30 ± 6 flinches 10 min^{-1}, $P < 0.05$). No significant reduction in the pain behavior was observed when Df1a-NH_2 or Df1a-OH was administered at 1 μM (40 pmoles in a 40 μl injection). Data are presented as mean ± SEM of $n = 5$ mice per group treated with Df1a and $n = 12$ mice in the control group.

3.7 Structure analysis of Df1a

The 3D structure of μ-TRTX-Df1a was modeled using the structure of β/ω-theraphotoxin-Tp1a (ProTx-I, PDB code 2M9L) as a template (Gui et al., 2014) (Figure 9A). The model obtained had a GMQE score of 0.91, with 82% of residues in the favored region of the Ramachandran plot. The structural model revealed Df1a adopts an ICK fold that is organized into two distinct faces; a hydrophobic patch surrounded by charged residues lies opposite a face comprised primarily of neutral hydrophilic residues face (Figure 9B). The hydrophobic patch is dominated by aromatic residues in Df1a, including the central W4, F5, W27 and W30 residues and the peripheral W32 and F34 residues. This is reminiscent of the hydrophobic patch present in the ProTx-I (Y4, W5, W27, W30 and F34), although there are significant differences including E17K, Q26G and W32G (Figure 9C). Nevertheless, the structural data suggest that these toxins share similar binding properties to $Na_V1.7$.

4. **Discussion**

Spider venoms have proven to be a rich source of peptides ligands that modulate Na_V channels (King, 2011). Their ability to target ion channels at allosteric binding sites often enhances target selectivity and opens up opportunities for new ion channel therapeutics. In the present work, we report the discovery and characterization of a new Na_V and Ca_V3 channel inhibitor named Df1a from the tarantula *Davus fasciatus*. Df1a belongs to NaSpTx Family 2, whose members contain an ICK motif and highly conserved N and C-termini. The closest orthologue of Df1a is the Na_V and Ca_V3 channel inhibitor ProTx-I (Middleton et al., 2002). However, ProTxI causes a reduction in peak current without altering channel inactivation, whereas Df1a has the dual effect of reducing peak current and slowing fast inactivation of some Na_V channel subtypes.

Electrophysiology using mammalian cells revealed that Df1a inhibits hNa_V with a rank order of potency 1.7>1.2>1.3>1.6>1.1>1.4>1.5, and hCa_V3 with a rank order 3.1>3.3>3.2. Interestingly, C-terminal amidation of Df1a increased potency by 1.7 to 4-fold for $hNa_V1.1$ to $hNa_V1.6$, 1.2 to 8.7-fold for $hCa_V3.1$ to $hCa_V3.3$, and remarkably by 32-fold for $hNa_V1.7$. The effect on $hNa_V1.7$ was also observed using two-electrode voltage clamp in oocytes; in this system C-terminal amidation increased potency against $Na_V1.7$ by 22-fold. C-terminal amidation has been reported to significantly increase the potency of other NaSpTx peptides. The amidated form of huwentoxin-IV, a toxin isolated from the spider *Haplopelma schmidti*, is 42-fold more potent against $Na_V1.7$ (Sermadiras et al., 2013). The C-terminally amidated form of ProTx-III, a toxin that we recently isolated from the spider *Thrixopelma pruriens*, is 4.6-fold more potent against $Na_V1.7$, and 8.9 and 3.5-fold more potent against $Na_V1.1$ and $Na_V1.3$, respectively (Cardoso et al., 2015). Although these peptides do not display favorable selectivity for key ion channels involved in complex disorders, the remarkable increase in potency of their C-terminal amide forms is important for the rational development of peptide drugs that target voltage-gated ion channels.

Among the ion channels studied in this work, $hNa_V1.3$, $hNa_V1.7$ and $hCa_V3.2$ are known to be involved in pain disorders. $hNa_V1.3$ is upregulated in dorsal root ganglion neurons during chronic constriction nerve injury and following axotomy (Dib-Hajj et al., 1999; Waxman et al., 1994). Lack of $Na_V1.7$ function induces insensitivity to pain (Cox et al., 2006), and a monoclonal antibody against $Na_V1.7$ suppresses inflammatory and neuropathic pain in mice (Lee et al., 2014). Altered T-type Ca^{2+} currents are involved in somatic and visceral pain signaling, and the hyperalgesia induced by L-cysteine was reported to be present in wild-type but not $Ca_V3.2$-knockout mice (Maeda et al., 2009; Nelson et al., 2007). These studies emphasize the potential of Df1a as a tool peptide to help guiding the development of novel drugs that simultaneously target Na_V and Ca_V channels involved in chronic pain states.

Patch-clamp studies revealed that Df1a alters the voltage-dependence of activation and inactivation of hNa_V channels. Other spider toxins belonging to NaSpTx2 and which alter the gating properties of Na_V channels are β-TRTX-Cm2a and μ-TRTX-Cj1a (Bosmans et al., 2006; Chen et al., 2009). Curiously, Df1a also slowed fast inactivation of $hNa_V1.1$, $hNa_V1.3$ and $hNa_V1.5$. A similar effect was observed for the spider toxin JZTX-XI, which slowed fast inactivation of TTX-R and TTX-S sodium channels (Liao et al., 2006; Tao et al., 2016), and for the spider toxin ProTx-II at $Na_V1.2$ to $Na_V1.5$ and $Na_V1.7$ channels (Xiao et al., 2010). However, ProTx-II induces persistent currents in $hNa_V1.7$ at saturating concentrations, while Df1a is a full inhibitor of Na_V channel currents irrespective of subtype. Interestingly, Df1a showed no changes in the voltage-dependence of activation and inactivation of $hNa_V1.7$ using two-electrode voltage clamp in oocytes. Differences in membrane composition between mammalian cells and oocytes that potentially influence how spider toxins bind to the $Na_V1.7$ channel could explain the effects observed (Henriques et al., 2016). Furthermore, for the two-electrode voltage clamp studies reported here, no β subunit was co-expressed with $Na_V1.7$, which could alter gating properties as well as toxin affinity to the channel. It was previously demonstrated that in oocytes, in the absence of the β1 subunit, fast inactivation of Na_V is slowed and steady-state inactivation altered by a ΔV_{50} of 6 mV (Shcherbatko et al., 1999). In this present study, the ΔV_{50} of $Na_V1.7$ steady-state inactivation observed in the presence and absence of the β1 subunit was 12 mV, which confirms the slowing in inactivation previously observed. Furthermore, in studies in which $Na_V1.2$ was expressed in oocytes, the spider toxin ProTx-II completely lost affinity to this channel in the presence of the β4 subunit, while the scorpion toxin TsVII showed potent activity over $Na_V1.2$ only in the absence of β4 (Gilchrist et al., 2013).

To further investigate the site of action of Df1a, we used a panel of $hNa_V1.7/K_V2.1$ chimeras (Klint et al., 2015). These experiments revealed that Df1a preferentially interacts with the DII voltage sensor of $hNa_V1.7$, and to a less extent with the DIII and DIV voltage sensors. The data also revealed that Df1a has no effect on $K_V2.1$, although its closest orthologue ProTx-I potent inhibits this potassium channel (Middleton et al., 2002). Previous reports have shown that inhibition of $Na_V1.7$ by spider toxins is mediated through interactions with the DII voltage sensor (Klint et al., 2015), whereas toxins that slow fast inactivation primarily interact with the DIV voltage sensor (Campos et al., 2008; Mitrovic et al., 2000; Rogers et al., 1996; Tao et al., 2016; Xiao et al., 2010). Similar studies performed with ProTx-II demonstrated interactions of this toxin with the DI, DII and DIV voltage sensors of $Na_V1.2$ (Bosmans et al., 2008), suggesting that DII and DIV interactions mediate the dual modulatory effects observed for both Df1a and ProTx-II. Df1a does not affect fast inactivation of $hNa_V1.7$, consistent with its more robust binding to the DII voltage sensor of this channel. In contrast, since Df1a does slow fast inactivation of $Na_V1.1$, $Na_V1.3$ and $Na_V1.5$, we speculate that the toxin interacts more avidly with the DIV voltage sensor in these Na_V channel subtypes. Although the chimeric channels provide useful insights into the binding sites for Df1a on Na_V channels, these interactions might differ among Na_V channel subtypes and/or in the complete Na_V voltage-sensor constructs.

Modeling of the Df1a structure revealed an ICK motif typical of spider toxins gating-modifiers (Klint et al., 2012). Furthermore, the structure of Df1a displayed surface similarities with the structure of ProTx-I (Gui et al., 2014) and three other spider toxins belonging to the NaSpTx Family 2 and inhibitors of K_V (κ-TRTX-Gr1a and κ-TRTX-Scg1a) and Ca_V (ω-TRXT-Gr1a) (Takahashi et al., 2000; Takeuchi et al., 2002; Wang et al., 2004). These displayed a conserved large hydrophobic patch surrounded by positively charged residues which is potentially involved in the interactions with the hydrophobic core of the cell membrane and the S3-S4 linker regions of the voltage-gated ion channels. The pharmacophore for ProTx-I interaction with $hNa_V1.2$ was established by alanine-scan (Gui et al., 2014), from which the key residues identified were found to be identical in Df1a, suggesting that these toxins possibly share a similar pharmacophore for Na_V channels. Further studies are required to elucidate pharmacophore for Df1a as well as identify residues that might enhance selectivity towards key channels subtypes and its potential as a lead for treating Na_V and Ca_V3-related disorders.

Finally, given the important role of Na_V channels in nociception, we tested the analgesic efficacy of Df1a in a rodent pain model in which nocifensive behavior is elicited by intraplantar administration of the Na_V activator OD1 (Cardoso et al., 2015; Deuis et al., 2016; Durek et al., 2013). Intraplantar administration of Df1a-NH_2 and Df1a-OH reduced the nocifensive behavior by 42% and 71%, respectively, suggesting that Df1a can effectively inhibit OD1 induced pain at peripheral sensory nerve endings in the skin. Although we have evidence Df1a inhibits Na_V and Ca_V3 channels involved in peripheral sensory pain, the exact targets of the observed analgesic effect remain to be fully elucidated. Interestingly, the Df1a C-terminal acid was less potent than the amide form at the human Na_V isoform co-expressed with β1, but more effective at reducing pain behaviours in a rodent pain model. This effect could be related to differences between the human and rodent ion channel isoforms and/or due to distinct expression and combinations of auxiliary β subunits *in vivo*, which could lead to altered sensitivities to Df1a (Gilchrist et al., 2013; Isom, 2001). Assessment of the analgesic potential of Df1a in disease-specific pain models will provide additional insight into the clinical potential of this peptide for the treatment of chronic pain.

In conclusion, we have characterized a new spider toxin named μ-TRTX-Df1a. Df1a is a potent Na_V and Ca_V3 channel inhibitor that in addition to shifting the voltage-dependence of activation and inactivation produces a prominent slowing in fast inactivation at specific Na_V channels subtypes. Channel inhibition *in vitro* was enhanced by C-terminal amidation of Df1a, but the C-terminal acid form showed better analgesic properties *in vivo*. The *in vivo* analgesic efficacy of Df1a suggests it might be a useful lead for the development of analgesics targeting Na_V-induced pain.

Author contributions:

Research conception and design: Cardoso, Lewis and King. Conduction of experiments, analysis and interpretation of data: Cardoso, Dekan, Smith, Vetter, Deuis and Herzig. Wrote manuscript: Cardoso, Lewis. Revised manuscript: Cardoso, Dekan, Deuis, Herzig, Alewood, King, Lewis.

Conflict of interest

The authors have no conflicts of interest

Acknowledgments

This work was supported by Australian Research Council (Linkage Grant to GFK, RJL and PFA and Future Fellowship to IV) and Australian National Health & Medical Research Council (Program Grant APP1072113 to RJL, GFK and PFA, and Principal Research Fellowships to RJL, GFK and PFA). We thank Dr Frank Bosmans (School of Medicine, Johns Hopkins University, MD, USA) for $hNa_V1.7/rK_V2.1$ chimeras, and Prof. Emmanuel Bourinet (Institute of Functional Genomics, Montpellier University, FR) and Prof. Edward Perez-Reyes (School of Medicine, University of Virginia, USA) for Cav3 cell lines. We thank Dr Alun Jones (Institute for Molecular Bioscience, The University of Queensland, QLD, Australia) for help with mass spectrometry. Access to the Australian Proteome Analysis Facility is facilitated by support from the Australian Government's National Collaborative Research Infrastructure Strategy.

References

Alexander SP, Catterall WA, Kelly E, Marrion N, Peters JA, Benson HE, *et al.* (2015). The Concise Guide to PHARMACOLOGY 2015/16: Voltage-gated ion channels. Br J Pharmacol 172**:** 5904-5941.

Amin AS, Klemens CA, Verkerk AO, Meregalli PG, Asghari-Roodsari A, de Bakker JM, *et al.* (2010). Fever-triggered ventricular arrhythmias in Brugada syndrome and type 2 long-QT syndrome. Neth Heart J 18**:** 165-169.

Arnold K, Bordoli L, Kopp J, & Schwede T (2006). The SWISS-MODEL workspace: a web-based environment for protein structure homology modelling. Bioinformatics 22**:** 195-201.

Bosmans F, Martin-Eauclaire MF, & Swartz KJ (2008). Deconstructing voltage sensor function and pharmacology in sodium channels. Nature 456**:** 202-208.

Bosmans F, Rash L, Zhu S, Diochot S, Lazdunski M, Escoubas P, *et al.* (2006). Four novel tarantula toxins as selective modulators of voltage-gated sodium channel subtypes. Mol Pharmacol 69**:** 419-429.

Campos FV, Chanda B, Beirao PS, & Bezanilla F (2008). Alpha-scorpion toxin impairs a conformational change that leads to fast inactivation of muscle sodium channels. J Gen Physiol 132**:** 251-263.

Cardoso FC, Dekan Z, Rosengren KJ, Erickson A, Vetter I, Deuis J, *et al.* (2015). Identification and characterization of ProTx-III [μ-TRTX-Tp1a], a new voltage-gated sodium channel inhibitor from venom of the tarantula *Thrixopelma Pruriens*. Mol Pharmacol 88**:** 291-303.

Catterall WA, Cestele S, Yarov-Yarovoy V, Yu FH, Konoki K, & Scheuer T (2007). Voltage-gated ion channels and gating modifier toxins. Toxicon 49**:** 124-141.

Catterall WA, Kalume F, & Oakley JC (2010). Na_V1.1 channels and epilepsy. J Physiol 588**:** 1849-1859.

Chen J, Zhang Y, Rong M, Zhao L, Jiang L, Zhang D, *et al.* (2009). Expression and characterization of jingzhaotoxin-34, a novel neurotoxin from the venom of the tarantula Chilobrachys jingzhao. Peptides 30**:** 1042-1048.

Chino N, Kubo S, Nishio H, Nishiuchi Y, Nakazato M, & Kimura T (2006). Chemical synthesis of human β-defensin (hBD)-1,-2,-3 and -4: Optimization of the oxidative folding reaction. Int J Pept Res Ther 12**:** 203-209.

Cox JJ, Reimann F, Nicholas AK, Thornton G, Roberts E, Springell K, *et al.* (2006). An SCN9A channelopathy causes congenital inability to experience pain. Nature 444**:** 894-898.

Curtis MJ, Bond RA, Spina D, Ahluwalia A, Alexander SP, Giembycz MA, *et al.* (2015). Experimental design and analysis and their reporting: new guidance for publication in BJP. Br J Pharmacol 172**:** 3461-3471.

DeLano WL (2002). The PyMOL Molecular Graphics System, Version 1.5.0.4 Schrödinger, LLC.

Deuis JR, Wingerd JS, Winter Z, Durek T, Dekan Z, Zimmermann K, *et al.* (2016). Analgesic Effects of GpTx-1, PF-04856264 and CNV1014802 in a Mouse Model of NaV1.7-Mediated Pain. Toxins 8**:** 78.

Dib-Hajj SD, Fjell J, Cummins TR, Zheng Z, Fried K, LaMotte R, *et al.* (1999). Plasticity of sodium channel expression in DRG neurons in the chronic constriction injury model of neuropathic pain. Pain 83**:** 591-600.

Durek T, Vetter I, Wang CI, Motin L, Knapp O, Adams DJ, *et al.* (2013). Chemical engineering and structural and pharmacological characterization of the alpha-scorpion toxin OD1. ACS Chem Biol 8**:** 1215-1222.

Errington AC, Stohr T, Heers C, & Lees G (2008). The investigational anticonvulsant lacosamide selectively enhances slow inactivation of voltage-gated sodium channels. Mol Pharmacol 73**:** 157-169.

Gilchrist J, Das S, Van Petegem F, & Bosmans F (2013). Crystallographic insights into sodium-channel modulation by the beta 4 subunit. Proceedings of the National Academy of Sciences of the United States of America 110**:** E5016-E5024.

Gui J, Liu B, Cao G, Lipchik AM, Perez M, Dekan Z, *et al.* (2014). A tarantula-venom peptide antagonizes the TRPA1 nociceptor ion channel by binding to the S1-S4 gating domain. Curr Biol 24**:** 473-483.

Henriques ST, Deplazes E, Lawrence N, Cheneval O, Chaousis S, Inserra M, *et al.* (2016). Interaction of Tarantula Venom Peptide ProTx-II with Lipid Membranes is a Prerequisite for its Inhibition of Human Voltage-gated Sodium Channel NaV1.7. J Biol Chem.

Herzig V, & Hodgson WC (2009). Intersexual variations in the pharmacological properties of *Coremiocnemis tropix* (Araneae, Theraphosidae) spider venom. Toxicon 53**:** 196-205.

Herzig V, & King GF (2015). The cystine knot is responsible for the exceptional stability of the insecticidal spider toxin ω-Hexatoxin-Hv1a. Toxins (Basel) 7**:** 4366-4380.

Herzig V, Wood DL, Newell F, Chaumeil PA, Kaas Q, Binford GJ, *et al.* (2011). ArachnoServer 2.0, an updated online resource for spider toxin sequences and structures. Nucleic Acids Res 39**:** D653-657.

Isom LL (2001). Sodium channel beta subunits: anything but auxiliary. Neuroscientist 7**:** 42-54.

Kaas Q, Yu R, Jin AH, Dutertre S, & Craik DJ (2012). ConoServer: updated content, knowledge, and discovery tools in the conopeptide database. Nucleic Acids Res 40**:** D325-330.

King GF (2011). Venoms as a platform for human drugs: translating toxins into therapeutics. Expert Opin Biol Ther 11**:** 1469-1484.

King GF, & Hardy MC (2013). Spider-venom peptides: structure, pharmacology, and potential for control of insect pests. Annu Rev Entomol 58**:** 475-496.

Klint JK, Senff S, Rupasinghe DB, Er SY, Herzig V, Nicholson GM, *et al.* (2012). Spider-venom peptides that target voltage-gated sodium channels: pharmacological tools and potential therapeutic leads. Toxicon 60**:** 478-491.

Klint JK, Smith JJ, Vetter I, Rupasinghe DB, Er SY, Senff S, *et al.* (2015). Seven novel modulators of the analgesic target $Na_V1.7$ uncovered using a high-throughput venom-based discovery approach. Br J Pharmacol 172**:** 2445-2458.

Lauria G, Ziegler D, Malik R, Merkies IS, Waxman SG, Faber CG, *et al.* (2014). The role of sodium channels in painful diabetic and idiopathic neuropathy. Curr Diab Rep 14**:** 538.

Lee JH, Park CK, Chen G, Han Q, Xie RG, Liu T, *et al.* (2014). A monoclonal antibody that targets a $Na_V1.7$ channel voltage sensor for pain and itch relief. Cell 157**:** 1393-1404.

Liao Z, Yuan C, Deng M, Li J, Chen J, Yang Y, *et al.* (2006). Solution structure and functional characterization of jingzhaotoxin-XI: a novel gating modifier of both potassium and sodium channels. Biochemistry 45**:** 15591-15600.

Liu M, & Wood JN (2011). The roles of sodium channels in nociception: implications for mechanisms of neuropathic pain. Pain Med 12 Suppl 3**:** S93-99.

Lovell SC, Davis IW, Arendall WB, 3rd, de Bakker PI, Word JM, Prisant MG, *et al.* (2003). Structure validation by Cα geometry: Φ, Ψ and Cβ deviation. Proteins 50**:** 437-450.

Maeda Y, Aoki Y, Sekiguchi F, Matsunami M, Takahashi T, Nishikawa H, *et al.* (2009). Hyperalgesia induced by spinal and peripheral hydrogen sulfide: evidence for involvement of Cav3.2 T-type calcium channels. Pain 142**:** 127-132.

Meisler MH, & Kearney JA (2005). Sodium channel mutations in epilepsy and other neurological disorders. J Clin Invest 115**:** 2010-2017.

Middleton RE, Warren VA, Kraus RL, Hwang JC, Liu CJ, Dai G, *et al.* (2002). Two tarantula peptides inhibit activation of multiple sodium channels. Biochemistry 41**:** 14734-14747.

Mitrovic N, George AL, Jr., & Horn R (2000). Role of domain 4 in sodium channel slow inactivation. J Gen Physiol 115**:** 707-718.

Moldovan M, Alvarez S, Romer Rosberg M, & Krarup C (2013). Axonal voltage-gated ion channels as pharmacological targets for pain. Eur J Pharmacol 708**:** 105-112.

Nelson MT, Woo J, Kang HW, Vitko I, Barrett PQ, Perez-Reyes E, *et al.* (2007). Reducing agents sensitize C-type nociceptors by relieving high-affinity zinc inhibition of T-type calcium channels. J Neurosci 27**:** 8250-8260.

Ragsdale DS, & Avoli M (1998). Sodium channels as molecular targets for antiepileptic drugs. Brain Res Brain Res Rev 26**:** 16-28.

Remme CA, & Bezzina CR (2010). Sodium channel (dys)function and cardiac arrhythmias. Cardiovasc Ther 28**:** 287-294.

Rogers JC, Qu Y, Tanada TN, Scheuer T, & Catterall WA (1996). Molecular determinants of high affinity binding of α-scorpion toxin and sea anemone toxin in the S3-S4 extracellular loop in domain IV of the Na^+ channel alpha subunit. J Biol Chem 271**:** 15950-15962.

Rogers M, Tang L, Madge DJ, & Stevens EB (2006). The role of sodium channels in neuropathic pain. Semin Cell Dev Biol 17**:** 571-581.

Sermadiras I, Revell J, Linley JE, Sandercock A, & Ravn P (2013). Recombinant expression and in vitro characterisation of active Huwentoxin-IV. PLoS One 8**:** e83202.

Shcherbatko A, Ono F, Mandel G, & Brehm P (1999). Voltage-dependent sodium channel function is regulated through membrane mechanics. Biophys J 77**:** 1945-1959.

Southan C, Sharman JL, Benson HE, Faccenda E, Pawson AJ, Alexander SP*, et al.* (2016). The IUPHAR/BPS Guide to PHARMACOLOGY in 2016: towards curated quantitative interactions between 1300 protein targets and 6000 ligands. Nucleic Acids Res 44**:** D1054-1068.

Takahashi H, Kim JI, Min HJ, Sato K, Swartz KJ, & Shimada I (2000). Solution structure of hanatoxin1, a gating modifier of voltage-dependent K(+) channels: common surface features of gating modifier toxins. J Mol Biol 297**:** 771-780.

Takeuchi K, Park E, Lee C, Kim J, Takahashi H, Swartz K*, et al.* (2002). Solution structure of omega-grammotoxin SIA, a gating modifier of P/Q and N-type Ca(2+) channel. J Mol Biol 321**:** 517-526.

Tao H, Chen X, Lu M, Wu Y, Deng M, Zeng X*, et al.* (2016). Molecular determinant for the tarantula toxin Jingzhaotoxin-I slowing the fast inactivation of voltage-gated sodium channels. Toxicon 111**:** 13-21.

Vetter I, Mozar CA, Durek T, Wingerd JS, Alewood PF, Christie MJ, *et al.* (2012). Characterisation of Na_V types endogenously expressed in human SH-SY5Y neuroblastoma cells. Biochem Pharmacol 83**:** 1562-1571.

Wang JM, Roh SH, Kim S, Lee CW, Kim JI, & Swartz KJ (2004). Molecular surface of tarantula toxins interacting with voltage sensors in K_V channels. J Gen Physiol 123**:** 455-467.

Waxman SG, Kocsis JD, & Black JA (1994). Type III sodium channel mRNA is expressed in embryonic but not adult spinal sensory neurons, and is reexpressed following axotomy. J Neurophysiol 72**:** 466-470.

Xiao Y, Blumenthal K, Jackson JO, 2nd, Liang S, & Cummins TR (2010). The tarantula toxins ProTx-II and Huwentoxin-IV differentially interact with human Na_V1.7 voltage sensors to inhibit channel activation and inactivation. Mol Pharmacol 78**:** 1124-1134.

Zhao J, Dupre N, Puymirat J, & Chahine M (2012). Biophysical characterization of M1476I, a sodium channel founder mutation associated with cold-induced myotonia in French Canadians. J Physiol 590**:** 2629-2644.

Table 1. Kinetics of current inhibition and recovery of $hNa_V1.3$ and $hNa_V1.7$ after application of μ-TRTX-Df1a.

Channel	Toxin	Concentration	K_{on}	K_{off}	K_d
		nM	$nM^{-1}s^{-1}$	s^{-1}	*nM*
$hNa_V1.3$	sDf1a-NH_2	3	$1.4 \pm 0.1 \times 10^{-3}$	0	0
		30	$2.9 \pm 0.7 \times 10^{-4}$	ND	ND
	sDf1a-OH	10	$1.5 \pm 0.2 \times 10^{-3}$	$8.8 \pm 1.5 \times 10^{-3}$	12.5 ± 1.3
		100	$1.6 \pm 0.3 \times 10^{-4}$	ND	ND
$hNa_V1.7$	sDf1a-NH_2	2	$1.3 \pm 0.2 \times 10^{-2}$	0	0
		20	$6.3 \pm 1.3 \times 10^{-4}$	ND	ND
	sDf1a-OH	60	$9.0 \pm 1.2 \times 10^{-5}$	0	0
		600	$2.1 \pm 0.2 \times 10^{-5}$	ND	ND

sDf1a-NH_2 was applied at 3 and 30 nM for $hNa_V1.3$ and 2 and 20 nM for $hNa_V1.7$, while sDf1a-OH was applied at 10 and 100 nM for $hNa_V1.3$ and 60 and 600 for $hNa_V1.7$, and sodium currents measured. The kinetics of inhibition and recovery of inhibition were determined from the *I*/*Imax* as function of time from traces shown in Figures 7A–H fitted to a single exponential fit. Values are from $n = 5$ independent experiments (mean ± SEM). ND = Not determined.

Figure legends

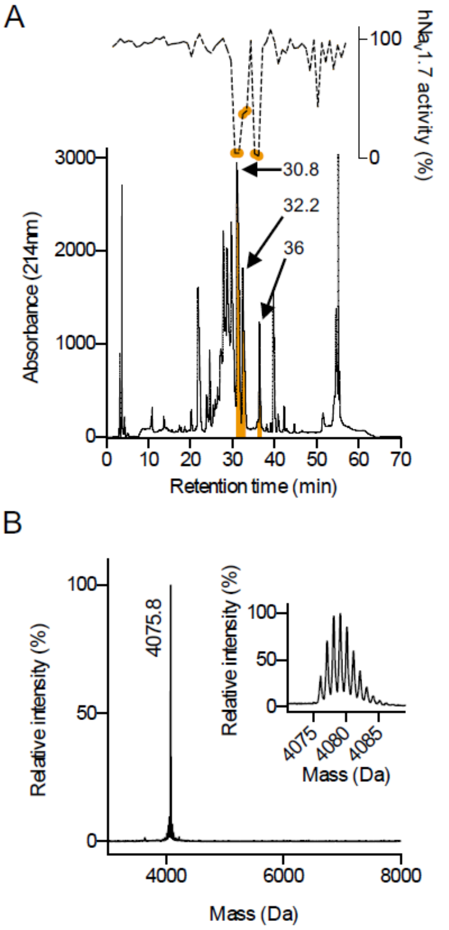

C

Toxin name	Sequence	Identity (%)	Activity
μ-TRTX-Df1a	-ECRWFLGGCSGGQTCCEHLVCHR-KHQWCVWDWSF-- 34*	100	Na$_V$, Ca$_V$3.1, Ca$_V$3.3
β/ω-TRTX-Tp1a	-ECRYWLGGCSAGQTCCKHLVCSR-RHGWCVWDGTFS- 35	73	Na$_V$, K$_V$2.1, Ca$_V$3.1
ω-TRTX-Hhn1a	-ECRWYLGGCSQDGDCCKHLQCHS-NYEWCVWDGT--- 33	64	Ca$_V$
ω-TRTX-Hh2a	-ECRWYLGGCSQDGDCCKHLQCHS-NYEWCVWDGTFSK 36	61	Ca$_V$
τ-TRTX-Pc1c	-ECRWYLGGCKEDSECCEHLQCHS-YWEWCLWDGSF-- 34*	61	TRPV1
U22-TRTX-Cj1a	-ECKWYLGDCKAHEDCCEHLRCHS-RWDWCIWDGTFG- 35	52	Unknown
U21-TRTX-Cj1c	-ECRWLFGGCEKDSDCCEHLGCRRTKPSWCGWDFTFGK 37*	57	Unknown
U21-TRTX-Cj1b	-ECRWLFGGCEKDSDCCEHLGCRRAKPSWCGWDFTFGK 37*	57	Unknown
τ-TRTX-Pc1b	GACRWFLGGCKSTSDCCEHLSCKM-GLDYCAWDGTF-- 35*	54	K$_V$2.1, TRPV1
τ/κ-TRTX-Pc1a	SECRWFMGGCDSTLDCCKHLSCKM-GLYYCAWDGTF-- 35*	50	K$_V$2.1, TRPV1
δ/κ-TRTX-Hm1a	-ECRYLFGGCSSTSDCCKHLSCRS-DWKYCAWDGTFS- 35	47	Na$_V$, K$_V$2.1, K$_V$4.1

Figure 1. Venom fractionation, activity screening on Na$_V$1.7, mass spectrometry and amino acids analysis of active fraction 36. (A) RP- HPLC of the *Davus fasciatus* crude venom (1 mg) was performed in Vydac218TP C18 using a three-step gradient of acetonitrile/0.05% trifluoroacetic acid (5-10% B for 5 min, 20-40% B for 40 min and 40-80% B for 5 min). Fractions were collected at 0.7 mL minute^{-1} and screened for Na$_V$1.7 inhibition using Calcium dye and FLIPR^{Tetra} instrument. Fractions eluted at 30.8, 32.2 and 36 min showed strong Na$_V$1.7 inhibition (orange shaded fractions). (B) MALDI-TOF mass spectrometry of

fraction 36 showing single predominant mass of 4075.8 Da. (C) Sequence identification and analysis of μ-TRTX-Df1a. Edman degradation analysis of the native toxin revealed a peptide with 34 residues containing 6 cysteines. The difference of masses between the native Df1a and predicted mass of the amino acids sequence revealed by Edman degradation indicates the presence of a C-terminal amidation in the native peptide. Sequence alignment of peptides toxins showing at least 47% identity in their amino acids sequence with Df1a. Identical residues are shown in blue and cysteine scaffold in red. The % of identity is shown relative to Df1a, and the activity reported for each peptide toxin is described in the far right column according to data sourced from the ArachnoServer database (Herzig et al., 2011). Asterisks denote C-terminal amidation. Df1a showed its highest identity with the toxin β/ω-TRTX-Tp1a (ProTx-I) isolated from the tarantula *Thrixopelma pruriens* (Middleton et al., 2002).

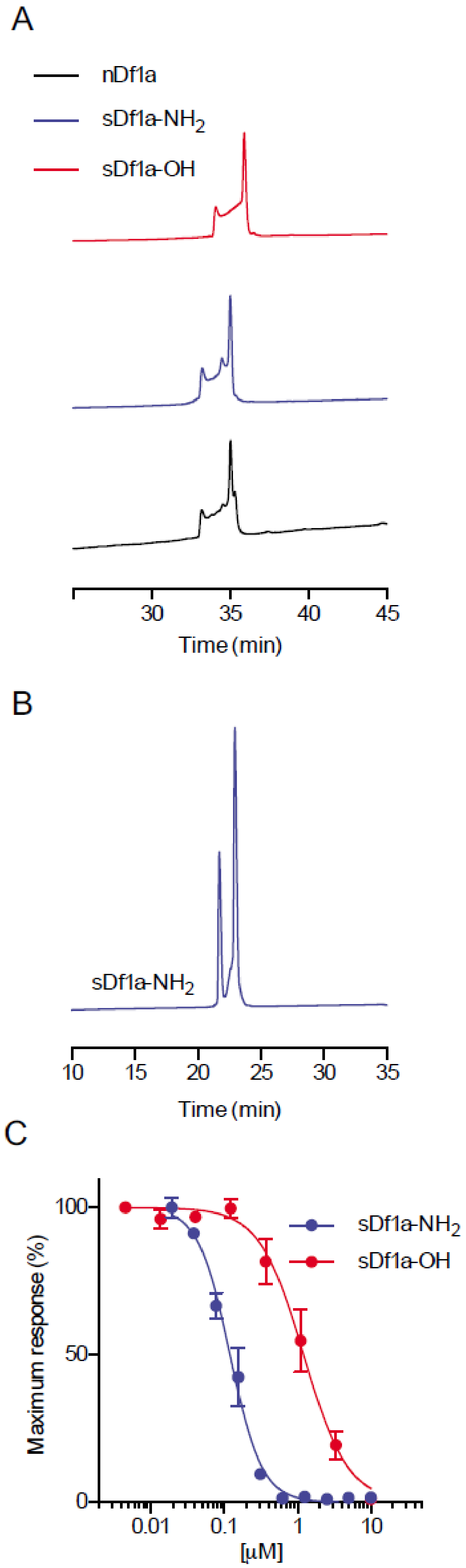
A
nDf1a
sDf1a-NH2
sDf1a-OH
30
35
40
45
Time (min)
B
sDf1a-NH2
10
15
20
25
30
35
Time (min)
C
100
50
0
Maximum response (%)
sDf1a-NH2
sDf1a-OH
0.01
0.1
1
10
[μM]

Figure 2. Comparison of the retention time of native μ-TRTX-Df1a and synthetic Df1a-NH_2 and Df1a-OH in HPLC. (A) Analytical RP-HPLC chromatograms of native amidated Df1a, synthetic Df1a-NH_2 and synthetic Df1a-OH. RP-HPLC was performed on a Shimadzu LC20AT system using a Thermo Hypersil GOLD C18 column (2.1 x 100 mm) heated at 40°C. Peptides were eluted using a gradient of 5–50% B over 45 min with a flow rate of 0.3 mL min^{-1}. Native Df1a and synthetic Df1a-NH_2 eluted both at 33.2 (minor peak) and 35.1 (major peak) min, while synthetic Df1a-OH eluted at 34.1 (minor peak) and 35.9 (major peak) min. (B) Analytical HPLC trace showing synthetic Df1a-NH_2 at 23°C. Lowering the temperature produced a deconvolution of the chromatogram resulting in only two peaks and disappearance of the unresolved portion between them observed at 40°C. (C) Activity of synthetic sDf1a-NH_2 and sDf1a-OH over $hNa_V1.7$ in SH-SY5Y cells determined using a fluorescent assay. The IC_{50} for $hNa_V1.7$ inhibitions were (in μM) 0.117 ± 0.006 and 1.24 ± 0.30 for sDf1a-NH_2 and sDf1a-OH, respectively. Data are presented as mean ± SEM, $n = 9$ independent experiments performed in 3 different days.

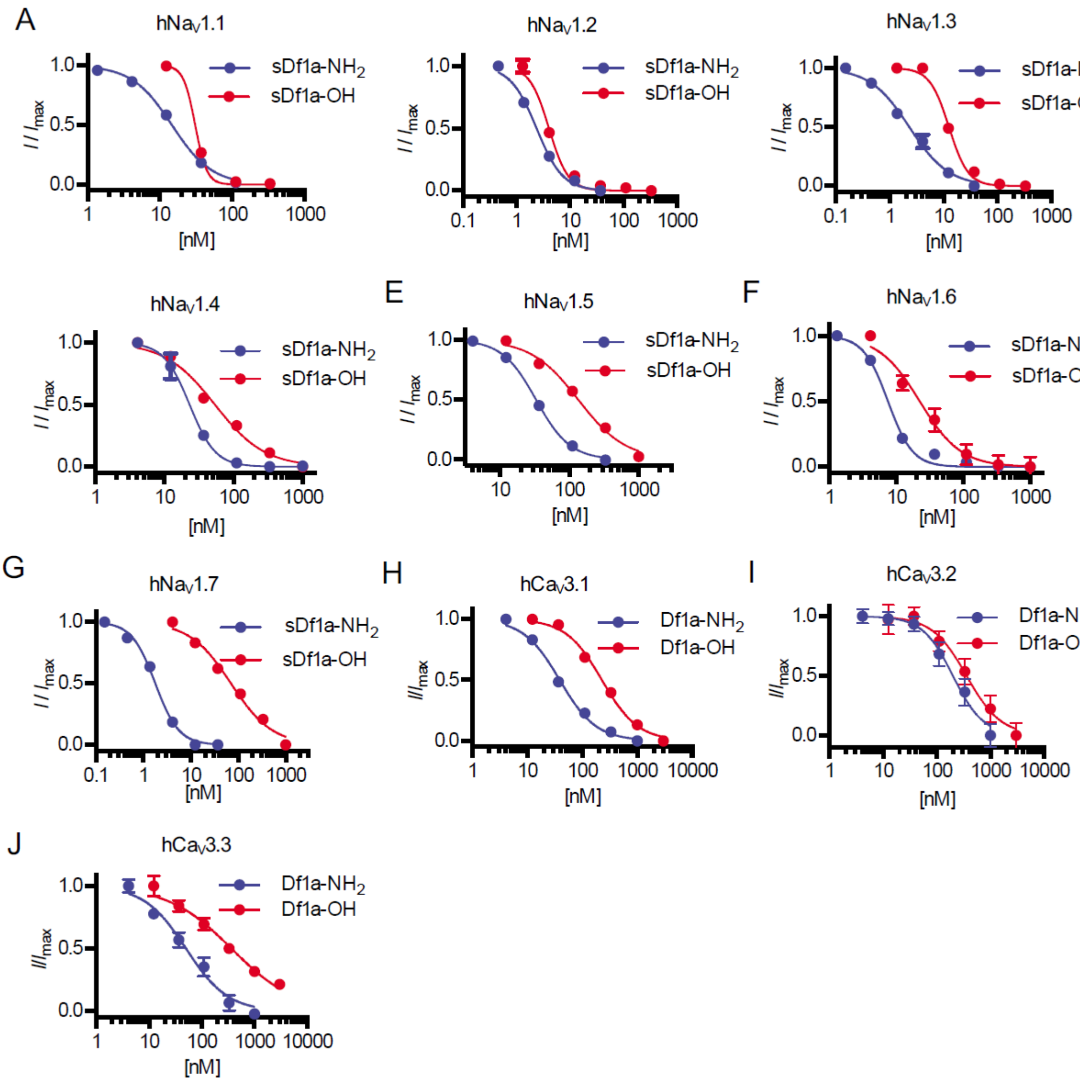

Figure 3. Inhibition of hNa_V and hCa_V3 subtypes by μ-TRTX-Df1a measured by automated patch clamp electrophysiology in QPatch 16X. Holding potential was –80 mV for hNa_V and –90 mV for hCa_V3. Na^+ currents were elicited by 20 ms voltage steps to 0 mV from a –120 mV conditioning pulse applied for 200 ms, and Ca^{+2} currents were elicited by 60 ms voltage steps to -30 mV from a –120 mV conditioning pulse applied for 60 ms. Representative concentration-response curves for inhibition of (A) $hNa_V1.1$, (B) $hNa_V1.2$, (C) $hNa_V1.3$, (D) $hNa_V1.4$, (E) $hNa_V1.5$, (F) $hNa_V1.6$, (G) $hNa_V1.7$, (H) $hCa_V3.1$, (I) $hCa_V3.2$ and (J) $hCa_V3.3$. The IC_{50} values calculated using I/I_{max} values and non-linear regression were (in nM) 14.3 ± 0.1 (n = 5) and 30.7 ± 2.2 (n = 6) for $hNa_V1.1$, 1.9 ± 0.5 (n = 5) and 3 ± 1.4 (n = 5) for $hNa_V1.2$, 3 ± 0.7 (n = 5) and 10 ± 1 (n = 8) for $hNa_V1.3$, 24 ± 1.8 (n = 5) and 53.6 ± 12 (n =6) for $hNa_V1.4$, 45.3 ± 6.8 (n = 5) and 125.6 ± 21 (n = 5) for $hNa_V1.5$, 7.6 ± 0.4 (n = 5) and 23 ± 2.9 (n = 7) for $hNa_V1.6$, 1.9 ± 0.08 (n = 6) and 60.5 ± 6.1 (n = 6) for $hNa_V1.7$, 44.6 ± 5.8 (n = 8) and 216 ± 28.1 (n = 7) for $hCa_V3.1$, 253 ± 45.7 (n = 6) and 371 ± 48.8 (n = 6) for $hCa_V3.2$

and 48.4 ± 7.2 (n = 5) and 460 ± 43.7 (n = 7) for $hCa_V3.3$, under application of sDf1a-NH_2 and sDf1a-OH, respectively. Data are represented as mean ± SEM from described n for independent experiments, one cell was considered per independent experiment.

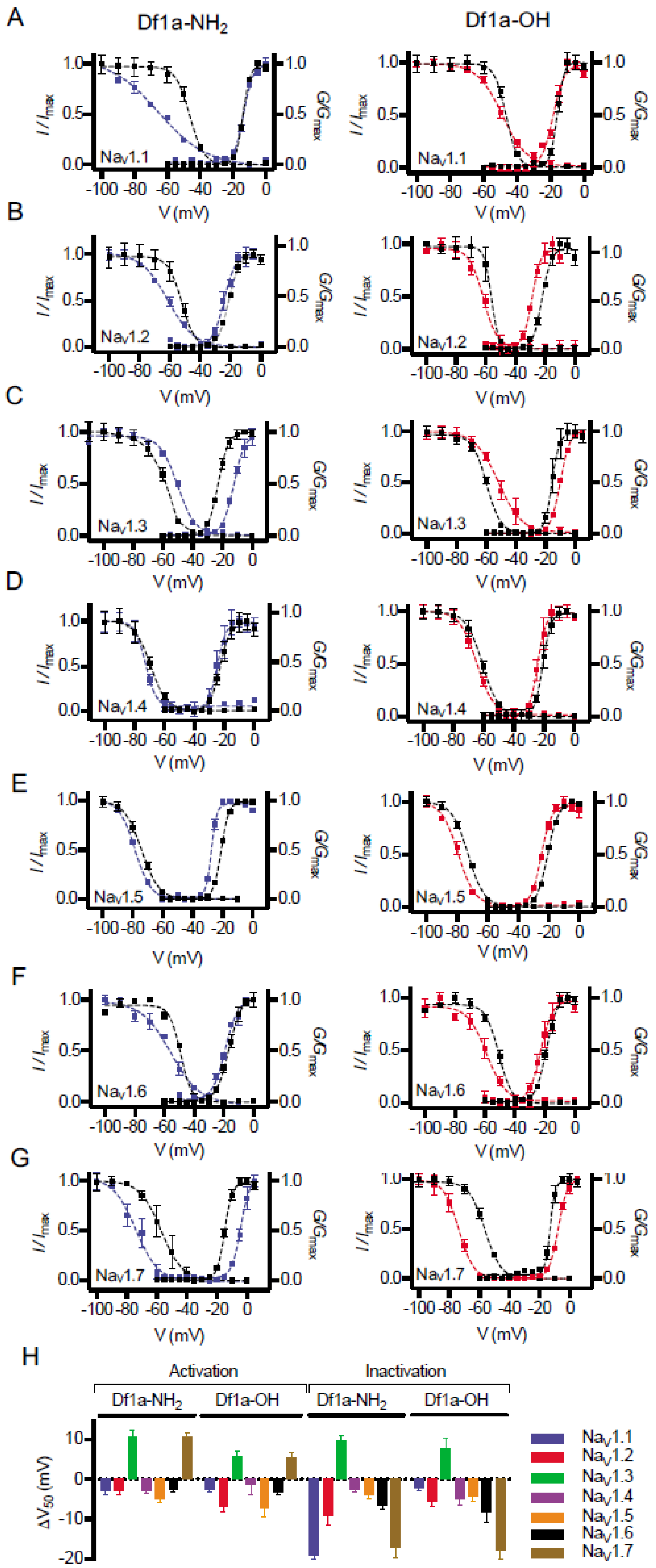
A
Df1a-NH2
Df1a-OH
Nav1.1
B
Nav1.2
C
Nav1.3
D
Nav1.4
E
Nav1.5
F
Nav1.6
G
Nav1.7
I / Imax
G/Gmax
V (mV)
H
Activation
Inactivation
Df1a-NH2
Df1a-OH
ΔV50 (mV)
Nav1.1
Nav1.2
Nav1.3
Nav1.4
Nav1.5
Nav1.6
Nav1.7

Figure 4. Modulation of the voltage dependence of hNa_V channels activation and inactivation gating in the presence of μ-TRTX-Df1a. Data (mean ± SEM, *n* = 5, one cell was considered per independent experiment) for (A) $hNa_V1.1$, (B) $hNa_V1.2$, (C) $hNa_V1.3$, (D) $hNa_V1.4$, (E) $hNa_V1.5$, (F) $hNa_V1.6$ and (G) $hNa_V1.7$ are plotted as G/G_{max} or I/I_{max}. Cells were held at –80 mV. μ-TRTX-Df1a C-terminal amide and acid were applied at respective IC_{50} concentration for each Na_V channel subtype as described in Figure 3 and Supporting Information Table S1. Steady state kinetics were estimated by currents elicited at 5 mV increment steps ranging from –110 to +80 mV. Conductance was calculated using $G = I/(V–V_{rev})$ in which *I*, *V* and V_{rev} are the current value, membrane potential and reverse potential, respectively. The voltage-dependence of fast inactivation was estimated using a double-pulse protocol where currents were elicited by a 20 ms depolarizing potential of 0 mV following a 500 ms pre-pulse at potentials ranging from –130 to –10 mV with 10 mV increments. Steady-state activation and inactivation V_{50} were determined by the Boltzmann equation. Both C-terminal acid and amide forms of sDf1a applied at respective IC_{50} concentrations modified the gating properties of hNa_V channels by shifting the voltage-dependence of activation and steady-state inactivation to more hyperpolarizing or depolarizing potentials. The ΔV_{50} was calculated, showing most of the voltage shifts towards more hyperpolarizing potentials, except for $hNa_V1.3$ and $hNa_V1.7$ that had some of these shifts to more hyperpolarizing potentials (Figure 4H).

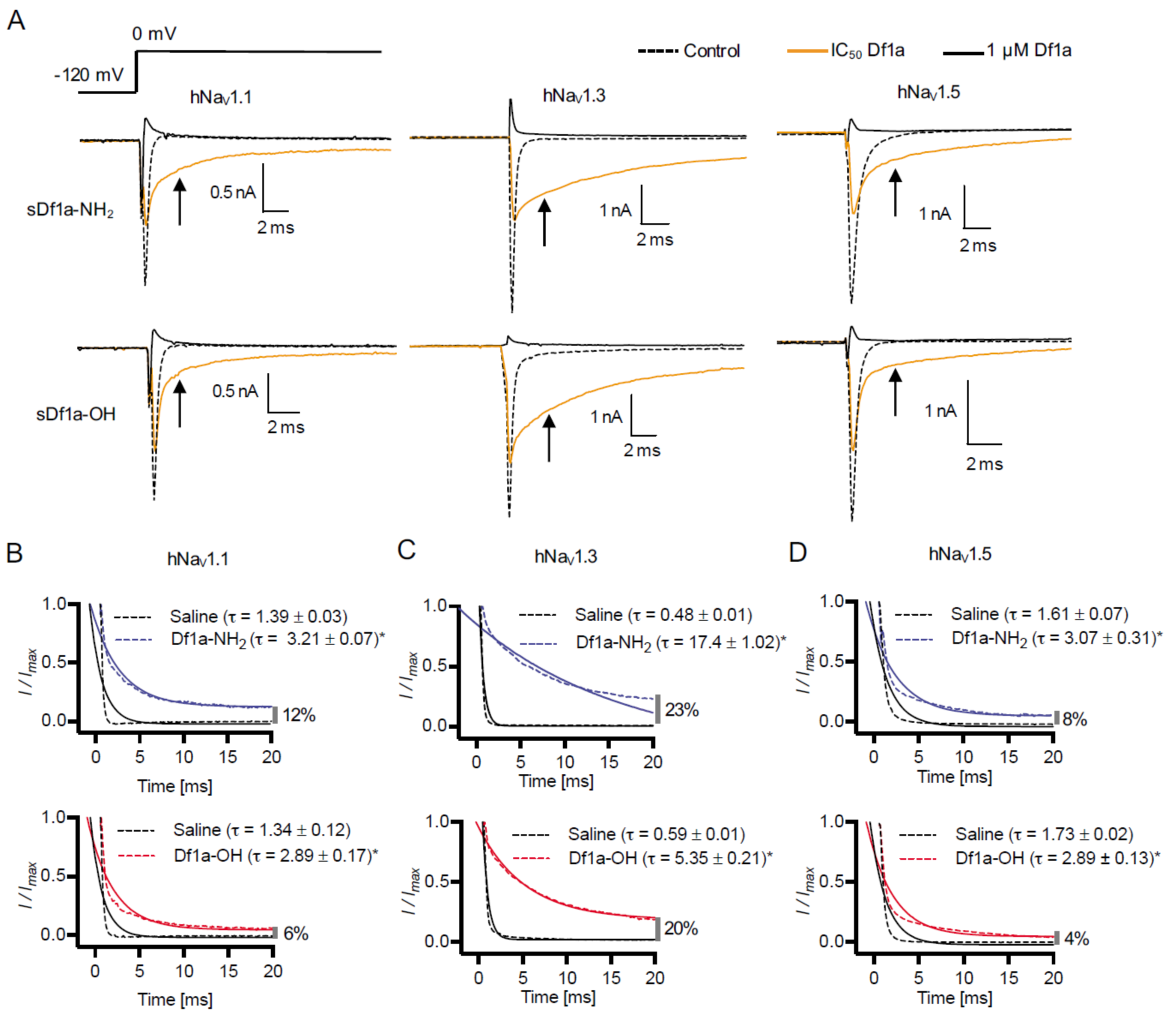

Figure 5. µ-TRTX-Df1a slows fast inactivation of hNa$_V$1.1, hNa$_V$1.3 and hNa$_V$1.5 along with peak current reduction under application of sDf1a-NH$_2$ or sDf1a-OH. The same effect is not observed in other hNa$_V$ subtypes tested, which presented only peak current reduction under application of sDf1a-NH$_2$ or sDf1a-OH (data not shown). Cells were held at –80 mV and Na^+ currents were elicited by 20 ms voltage steps to 0 mV from a –120 mV conditioning pulse applied for 200 ms. (A) Representative traces of hNa$_V$1.1, hNa$_V$1.3 and hNa$_V$1.5 in the presence of sDf1a-NH$_2$ and sDf1a-OH. Cells were applied with the correspondent IC$_{50}$ (black traces) and 1 µM sDf1a (gray trances) for each Na$_V$ subtype and incubated for 5 min before depolarization at 0 mV. No toxin controls are represented in dashed traces. Current traces showing the slowing in fast inactivation are featured by arrows. The slowing of fast inactivation at 5 ms after application of 0 mV was plotted against the log scale of various concentrations of Df1a, and maximum slowing in inactivation evaluated. (B-D) hNa$_V$1.1, hNa$_V$1.3 and hNa$_V$1.5 inactivation decay time constant (τ) and percentage of remaining currents were calculated in the presence of respective IC$_{50}$ concentrations of Df1a for each

channel subtype. Blue traces represent the time constant (τ) in the presence of Df1a-NH_2 and red traces in the presence of Df1a-OH. Remaining currents (%) are described in the far right of the x-axis at each graph. Remarkable slowing of fast inactivation is observed for the subtype $Na_V1.3$ in the presence of Df1a, which also displayed the highest percentage of remaining currents at 20 ms. Data are presented as mean ± SEM from $n \geq 5$ independent experiments for each ion channel assayed, one cell was considered per independent experiment (see Supporting Information Table S1).

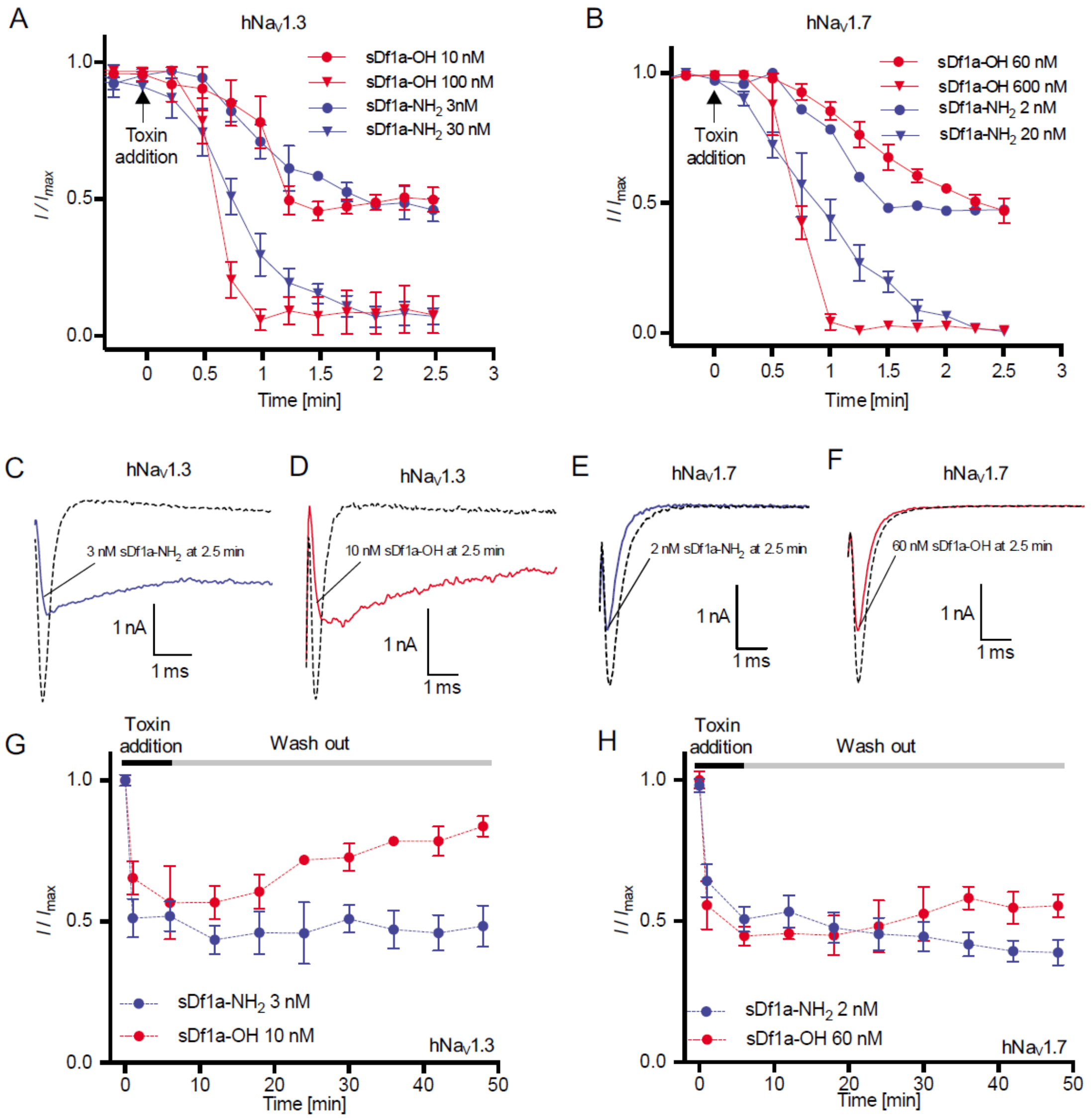

Figure 6. Kinetics of hNa$_V$ currents inhibition and recovery in the presence of µ-TRTX-Df1a. Cells were maintained at a holding potential –80 mV and Na$^+$ currents elicited by 20 ms voltage steps to 0 mV from a –120 mV conditioning pulse applied for 200 ms. (A) For on-rates, Na$^+$ currents were recorded every 15 seconds during 15 min after toxin addition. The on-rates for hNa$_V$1.3 were 4.34 and 2.03 min at 3 and 30 nM sDf1a-NH$_2$, respectively, and 1.14 and 1.13 min at 10 and 100 nM sDf1a-OH, respectively. (B) For hNa$_V$1.7, the on-rates were 0.64 and 1.32 min at 2 and 20 nM sDf1a-NH$_2$ and 3.06 and 1.32 min at 60 and 600 M sDf1a-OH, respectively. (C-F) Representative Na$^+$ current traces after 2.5 min incubation with Df1a along to consecutive pulses of 0 mV with 15 seconds intervals. A persistent slowing in fast inactivation associated to peak current reduction was observed for hNa$_V$1.3 in the presence of (C) 3 nM sDf1a-NH$_2$ and (D) 10 nM sDf1a-OH, while for hNa$_V$1.7, only peak

reduction is observed in the presence of (E) 2 nM sDf1a-NH_2 and (F) 60 nM sDf1a-OH. (G-H) For the wash-out of sDf1a-NH_2 and sDf1a-OH over $hNa_V1.3$ and $hNa_V1.7$, cells were incubated for 10 min with Df1a and Na^+ currents assessed at 5 min intervals during saline washes. The inhibition by sDf1a-OH at IC_{50} concentration is reversible only in the $hNa_V1.3$ subtype, while for sDf1a-NH_2 over $hNa_V1.3$ and $hNa_V1.7$, and sDf1a-OH over $hNa_V1.7$ the inhibition remained quasi-irreversible under applied experimental conditions at up 50 min recording. The K_{on}, K_{off} and K_d were calculated using $K_d = K_{off}/K_{on}$ (nM), where $K_{off} = 1/\tau_{off}$ (s^{-1}) and $K_{on} = (1/\tau_{on} - K_{off})/[toxin]$ ($nM^{-1}S^{-1}$). Data are presented as mean ± SEM, n = 5 independent experiments for each condition assayed, one cell was considered per independent experiment.

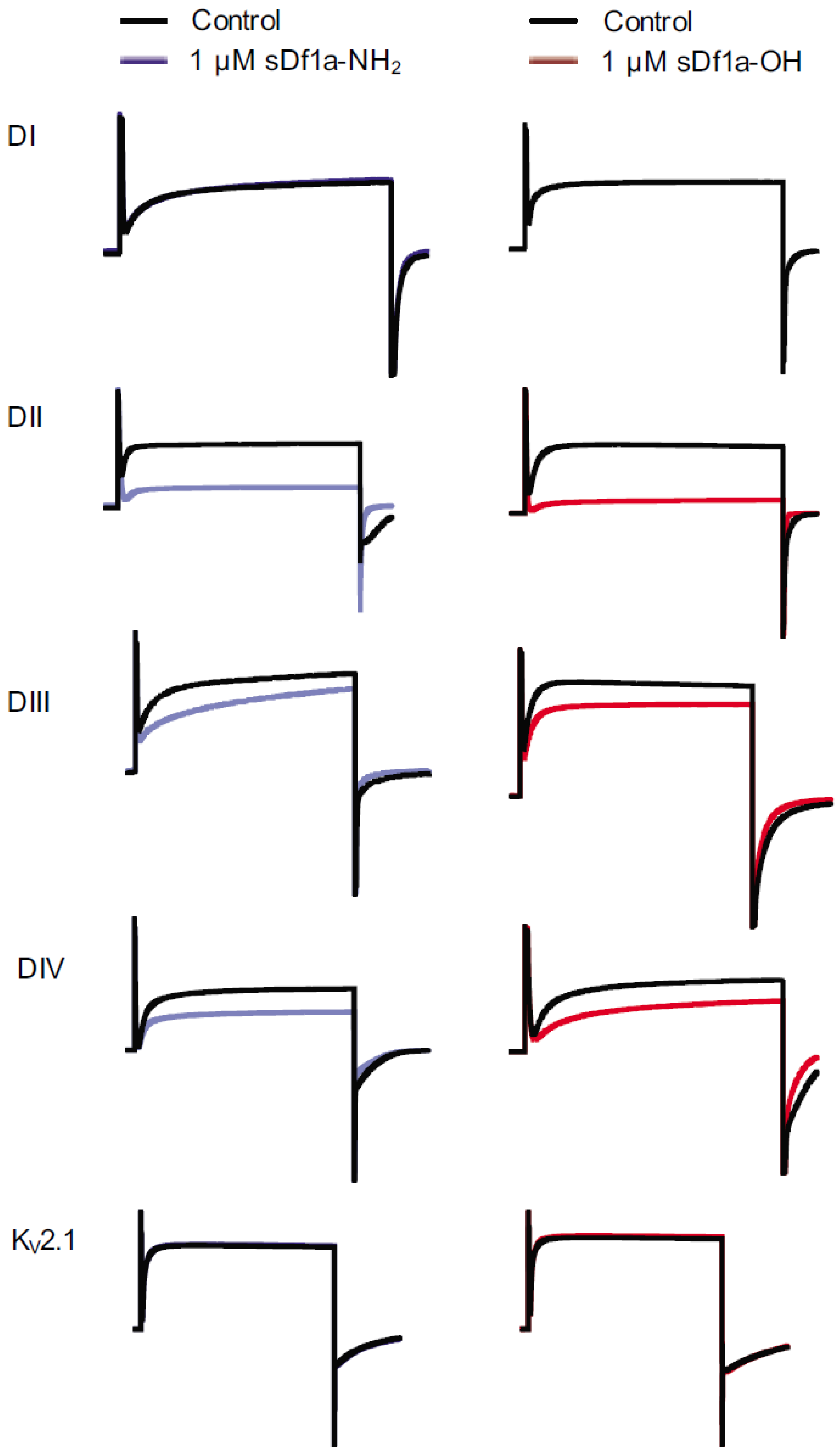
Control
1 μM sDf1a-NH2
Control
1 μM sDf1a-OH
DI
DII
DIII
DIV
KV2.1

Figure 7. Binding sites of μ-TRTX-Df1a over $hNa_V.7$. Chimeras $hNa_V1.7/rK_V2.1$ containing the paddles S3-S4 from DI-DIV from $Na_V1.7$ were used to explore the binding site of Df1a over $Na_V1.7$. Potassium currents elicited by depolarization to +70 mV. The currents are shown before and after addition of 1 μM Df1a toxin. sDf1a (both C-terminally acid and amide) preferentially binds to S3-S4 loop region in DII of $Na_V1.7$, followed by DIII and DIV. Df1a (C-terminally acid and amide) had no effect on wild-type $rK_V2.1$ at up to 1 μM. Data are from *n* = 5 independent experiments for each condition assayed, one oocyte was considered per independent experiment.

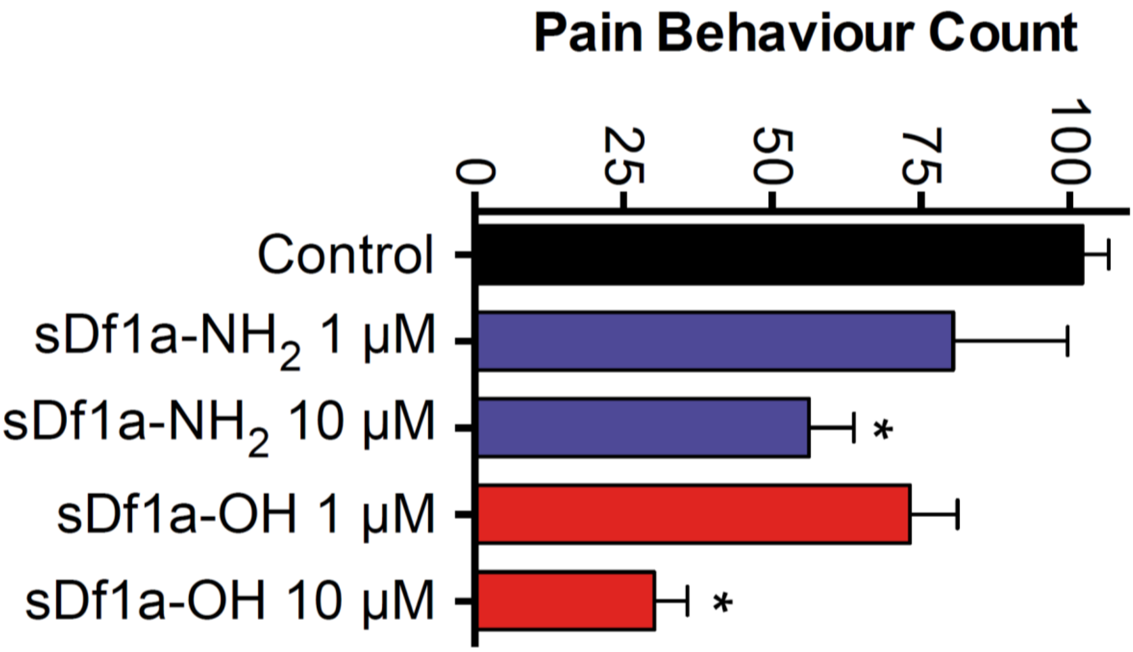

Figure 8. Antinociceptive effects of μ-TRTX-Df1a. (A) Intraplantar injection of the $Na_V1.7$ activator OD1 (300 nM) led to rapid development of nocifensive behavior in mice. This spontaneous pain behavior, measured by the number of paw licks and flinches, was attenuated in a concentration dependent manner by co-administration of sDf1a-OH at 1 and 10 μM, and sDf1a-NH_2 at 10 μM but not at 1 μM. Data are presented as mean ± SEM of n = 5 mice per group treated with Df1a and n = 12 mice in the control group, *$P < 0.05$.

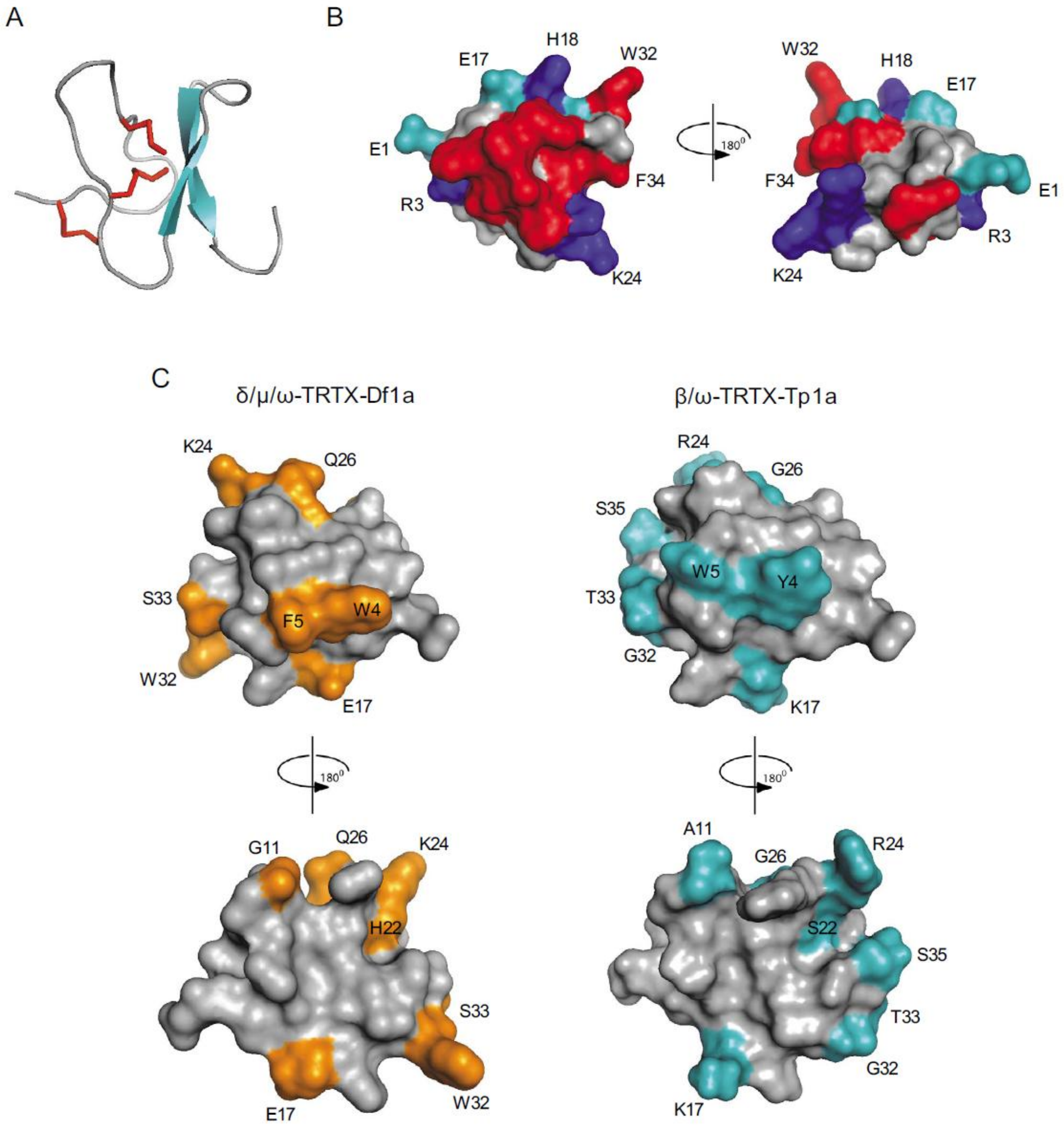

Figure 9. Molecular modeling and structural features of μ-TRTX-Df1a. The three dimensional structure of Df1a was calculated using the NMR structure of β/ω-theraphotoxin-Tp1a (ProTx-I) (Gui et al., 2014). (A) Cartoon model showing beta-sheet (cyan) and Cys-bridges (red) of a typical ICK peptide. (B) Surface representation of Df1a structure with 180° rotation shown in cyan: negatively charged, blue: positively charged and red: hydrophobic residues (aromatics). Residues present in these regions are labeled (E1, R3, E17, H18, K24, W32 and F34). (C) Comparison of the structures of Df1a and ProTx-I. Highlighted in orange and cyan are the differences in amino acids residues between these toxins, respectively. These residues are W4Y, F5W, G11A, E17K, H22S, K24R, Q26G, W32G, S33T for Df1a and ProTx-I, respectively, and S35 present only in ProTx-I. Structures are shown in two orientations, rotated by 180°.